Study on Multiphase Phenomena in Oil Production at a Pore Scale by Microtomography

March 2015

Arief Setiawan

Acknowledgements

Completion of this doctoral dissertation was possible with the support of several people. I would like to express my sincere gratitude to all of them. First of all, I am extremely grateful to my advisor Prof. Tetsuya Suekane for the continuous support of my study and research, for his patience, motivation, enthusiasm, and immense knowledge. His guidance helped me in all the time of research and writing of this dissertation. I could not have imagined having a better advisor and mentor for my study. I thank Prof. Yoshihiro Deguchi for the academic support and the facilities provided in The University of Tokushima. I also thank Prof. Koji Kusano for his help. The dissertation would not have come to a successful completion, without the help I received from the staff of the Faculty of Engineering.

I thank my fellow labmates in The University of Tokushima and Tokyo Institute of Technology. Also I thank my Indonesian friends in The University of Tokushima and Tokyo Institute of Technology. Last but not the least, I would like to thank my family: my parents Rivai Trimo and Tri Hidayati, for supporting me financially and spiritually throughout my life.

Arief Setiawan

January 2015, Tokushima, Japan

TABLE OF CONTENTS

1 INTRODUCTION

1.1 Background

Economic development over the past century was a result of relatively cheap and abundant oil-based energy. After the production peak, as supplies decline and prices rise, the world will have to use less fossil fuel and find alternate sources of energy. Some options are nuclear power, hydro-electricity, wind, tide, solar, geothermal, etc. Unfortunately, none of them offers cheap and convenient or as oil. Because of that reason, energy crisis is only matter of time. Fossil fuel continues to play a very important role in our energy supply and gives contribution approximately one third of total energy suppy.

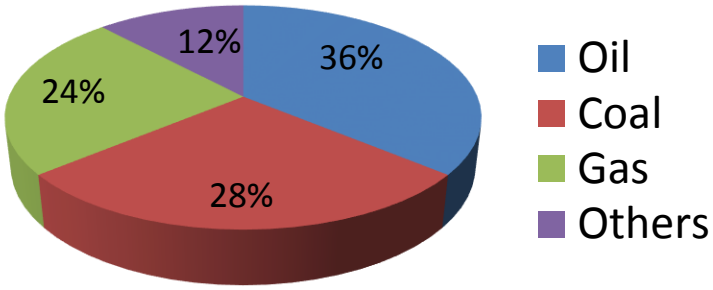

Fig. 1.1 World Primary Energy Consumption by Fuel Type, 2006 (BP Statistical Review of World Energy 2007)

Oil is stored inside porous rocks thousand meters under the ground, we call it oil reservoir. Potential reservoir is a rock has enough porosity and permeability that fluid can flow through it. Most rocks, in particular sandstones and conglomerates, is potential reservoir eventhough the amount of pore space may not be very much. Most sandstone reservoirs tend to be water-wet or intermediate-wet, whereas most carbonate reservoirs tend to be intermediate or oil-wet (Lake, 1989). Because oil is stored inside porous rock, it needs special technique to extract it. Generally, recovery of oil can be explained into 3 steps,

- Primary recovery

In this stage, driving forces of oil extraction are mainly natural mechanism including expansion of the natural gas at the top of the reservoir. Recovery factor during the primary recovery stage is typically 5-15%.

- Secondary recovery

In this stage, the oil extraction process is not depends on natural force, but external energy applied into reservoir in the form of injecting fluids to increase reservoir pressure. The most

common is water injection into oil reservoir called as water flooding process. On average, the recovery factor after primary and secondary oil recovery is between 35% – 45%

- Tertiary recovery

In this stage, some actions are applied into oil reservoir to increase oil mobility results in higher oil recovery. Some of the popular methods are surfactant injection, microbial injection, steam injection, etc. The biggest issue in this stage is economical issue, because sometime the oil production cost for applying tertiary recovery method is higher than the the value of additional oil that can be extracted.

Up to this time, oil production is an inefficient process. Even though we have more than 150 years development history, during the primary recovery and the application of water flooding, at least 50% of oil remains in the reservoir (Blunt et al. 1993). During the oil production, extraction of oil always followed by migration of water contained in oil reservoir. During this migration, the invasion of water may cut oil continuity causing oil entrapment. This phenomena also happen frequently when we applied water flooding process. Waterflooding is an oil production scheme usually applied to maintain reservoir pressure and can also be used as sweeping agent that push oil toward the production well. In some oil reservoirs, water covers the surface of porous rock more easily than oil. Therefore, water forms the wetting phase (WP) and oil forms the nonwetting phase (NWP). During waterflooding, water is forced into the reservoir from an injection well, invading pores previously occupied by oil and water; this is called forced imbibition. Fig. 1.2 shows the illustration of cross sectional view of oil reservoir. We can see that during the extraction process, oil is not only sucked by pump in production well, but also there is an external force that push oil toward production well keeping internal pressure and acts as sweeper. During water flooding process, there is a possibility that oil continuity will be disrupted and oil is trapped inside pore space. Once the oil flow is disrupted, capillary forces between the water and oil holds the oil blob in the pore space, making extraction difficult. Even if a surfactant is injected to relax the tension, some oil remains trapped and cannot be extracted (Porzucek and Ramirez 1990). Oil company did so much efforts to produce trapped oil, but lack of knowledge about what actually happen in oil reservoir becaome major issue. Because of that reason, there are many old oil production wells are abandoned because remaining oil is trapped inside reservoir and it cannot be extracted economically. Based on this fact, we still have opportunity to produce more oil if we develop oil production process that makes us possible to extract trapped oil economically and prevent oil entrapment during the process.

Improving production efficiency is one of the key solutions for overcoming the energy crisis; at least for the next few decades.

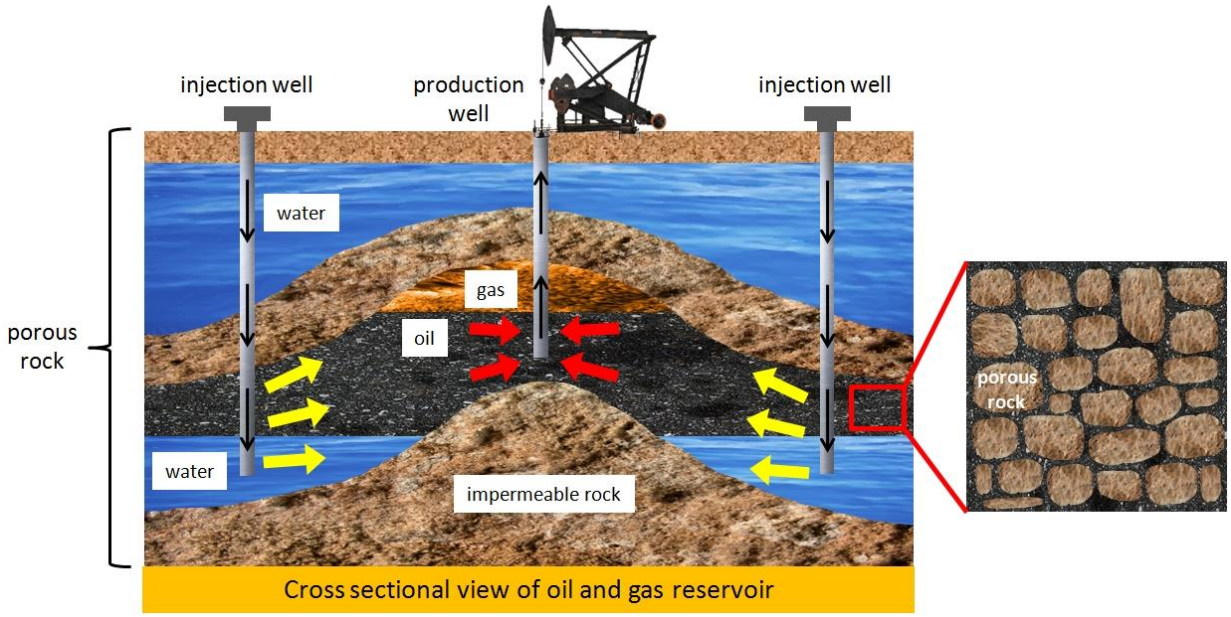

Fig. 1.2 Cross sectional view of oil reservoir

Developing an efficient waterflooding scheme is a difficult task; therefore, an understanding of the multiphase interaction in porous rock is necessary from a microscopic viewpoint. Until now, no one know what actually happen inside oil reservoir thousand meters underneath the ground. Moreover no one knows how to prevent such oil entrapment and how oil interact with injected fluid. Multiphase flow phenomena in porous medium have been observed from a microscopic viewpoint by using a micromodel (Chang et al. 2009; Jamaloei et al. 2010; Lenormand 1990) or a simulation (Blunt and King 1992; Kang et al. 2004, Lenormand et al. 1988). However, micromodels usually describe the process two dimensionally, and the simulation generally needs precise determination of many parameters. Although the observation of a two-dimensional (2-D) multiphase phenomena is less expensive and easier to work with, a three-dimensional (3-D) observation describes the flow phenomena more realistically because it contains more interconnections (Jerauld and Salter 1990). An additional scheme is required to study the process more realistically. Pore-scale observation in 3-D porous media is a solution because pore-scale processes govern the fundamental behavior of the multiphase flow phenomena in porous media (Al-Raoush and Willson 2005); the multiphase flow characteristics of this phenomena can vary (Blunt

1995). Because of the development of microfocused X-ray CT scanner technology, the nondestructive visualization of the phenomenon is possible (Kumar et al. 2010), and the application of this technology is a critical first step for understanding fluid transport in porous media.

1.2 Objectives

Utilizing microfocused X-ray CT scanner, water flooding process and oil trapping mechanism in artificial porous medium in laboratory-scale can be observed clearly. To impove the accuracy of the images, new visualization scheme was developed by carefully select each phase involved in this reseach so that the X-ray broadening effect can be minimalized. By varying the injection direction (upward and downward), more comprehensive description of water flooding process can be made. Comparing those data, the dominant mechanism occurs in oil trapping process in each case can be obtained. To make observation more realistic compared to actual oil reservoir, water flooding was also conducted with variation of porous medium wettability. Different wettability may shows different phenomena during water invasion process and oil trapping phenomena.

In actual oil reservoirs, connate water is usually found. Some studies suggest that connate water adds additional perturbations to the displacement front, causing more irregular water fingering in oil–wet porous medium during water flooding (Paterson et al., 1984; Jamaloei et al., 2010). During water flooding, the connate water is displaced from the core and connate water bank accumulation is formed in front of the injected water, thus affecting invasion patterns (Graue et al., 2012). Connate water displaces in a piston-like displacement during spontaneous imbibition (Graue and Ferno, 2011). The effect of connate water was also observed in this research. How connate water affects residual oil saturation and local velocity of oil is also discussed.

Injection of sweeping agent which is usually conducted by oil companies during tertiary production process after oil has been trapped after water flooding is not capable of producing 100% trapped oil. In order to release those trapped oil blobs from pore space, sweeping agent (surfactant, bacteria, steam, etc) need to make a contact with the trapped oil blobs. To understand why injection of sweeping agent cannot produce 100% of trapped oil, the flow phenomena around trapped oil blobs were observed in this research.

2 OBSERVATION OF WATER INVASION AND OIL TRAPPING MECHANISM

2.1 Background

In secondary stage of the oil production, oil production always followed by migration of water contained in oil reservoir. During this migration, the invasion of water may cut oil continuity causing oil entrapment. This phenomena also happen frequently when we applied water flooding process. Until now, there is little information about what actually happen inside oil reservoir thousand meters underneath the ground. Moreover there is no developed scheme to prevent such oil entrapment. Because of that reason, we tried to observe water-oil flow phenomena by making artificial oil reservoir and reconstruct the phenomena while scanning the process by using microfocused X-Ray CT scanner. Packed glass beads was used as artificial reservoir because of its regular shapes that make observation become easier.

Invasion of water into pore previously occupied by oil in water-wet porous medium is usually called as imbibition. The imbibition of brine into the reservoir rock is an important issue when producing oil from fractured reservoirs, especially when the reservoir rock has low permeability (Morrow and Mason 2001). However, there is little information on this process, especially from a microscopic viewpoint. Until now, imbibition has been observed from a microscopic viewpoint by using a micromodel (Chang et al. 2009; Jamaloei et al. 2010; Lenormand 1990) or a simulation (Blunt and King 1992; Kang et al. 2004, Lenormand et al. 1988). However, micromodels usually describe the imbibition process two dimensionally, and the simulation of imbibition generally needs precise determination of many parameters. Although the observation of a two-dimensional (2-D) imbibition process is less expensive and easier to work with, a three-dimensional (3-D) imbibition process describes the flow phenomena more realistically because it contains more interconnections (Jerauld and Salter 1990).

An additional scheme is required to study the process more realistically. Pore-scale observation in 3-D porous media is a solution because pore-scale processes govern the fundamental behavior of the multiphase flow phenomena in porous media (Al-Raoush and Willson 2005); the imbibition characteristics of this phenomena can vary (Blunt 1995). Because of the development of microfocused X-ray CT scanner technology, the

nondestructive visualization of the phenomenon is possible (Kumar et al. 2010), and the application of this technology is a critical first step for understanding fluid transport in porous media.

2.2 Experiments

2.2.1 Experimental Scheme

We used Comscantechno Co., ScanXmate-RB090SS as micro focused x-ray CT scanner to analyze the oil trapping mechanism and the water fingering phenomenon occured during imbibition as shown in Fig. 2.1. The image resolution depended on the distances among the X-ray source, detector, and object. The image produced by the X-ray CT scanner was a gray-scale image. To clearly observe the multiphase phenomena, we used phases with different X-ray absorption properties so that the brightness of each phase in the gray-scale image was distinct and could be differentiated solely by determining its minimum and maximum brightness.

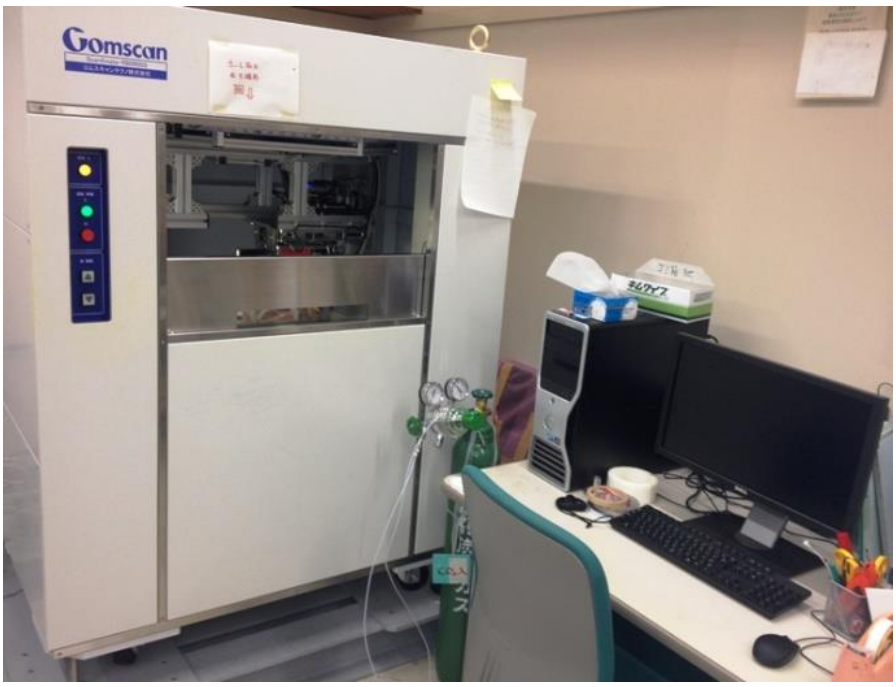

Fig. 2.1 Micro focused X-ray CT scanner (Comscantechno Co., ScanXmate-RB090SS)

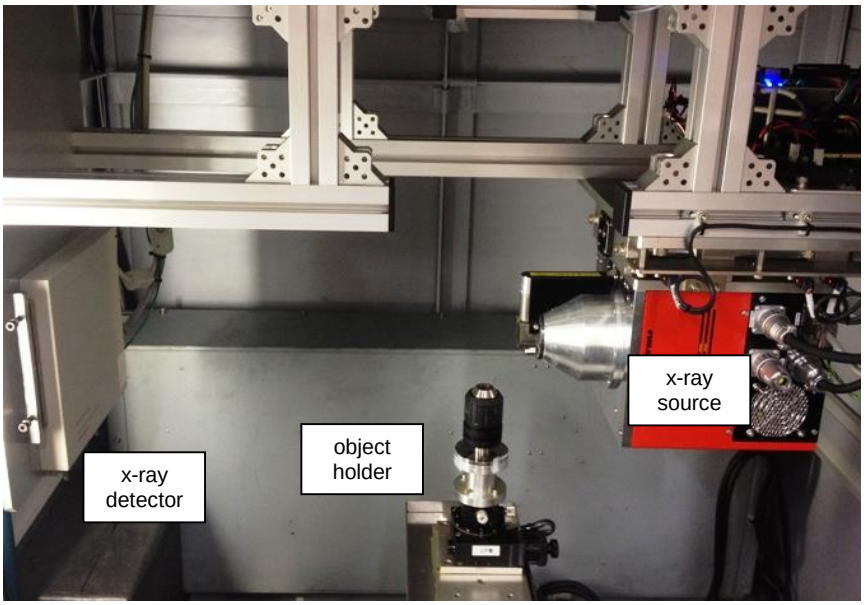

Fig. 2.2 Inside view of micro focused X-ray CT scanner (Comscantechno Co., ScanXmate-RB090SS)

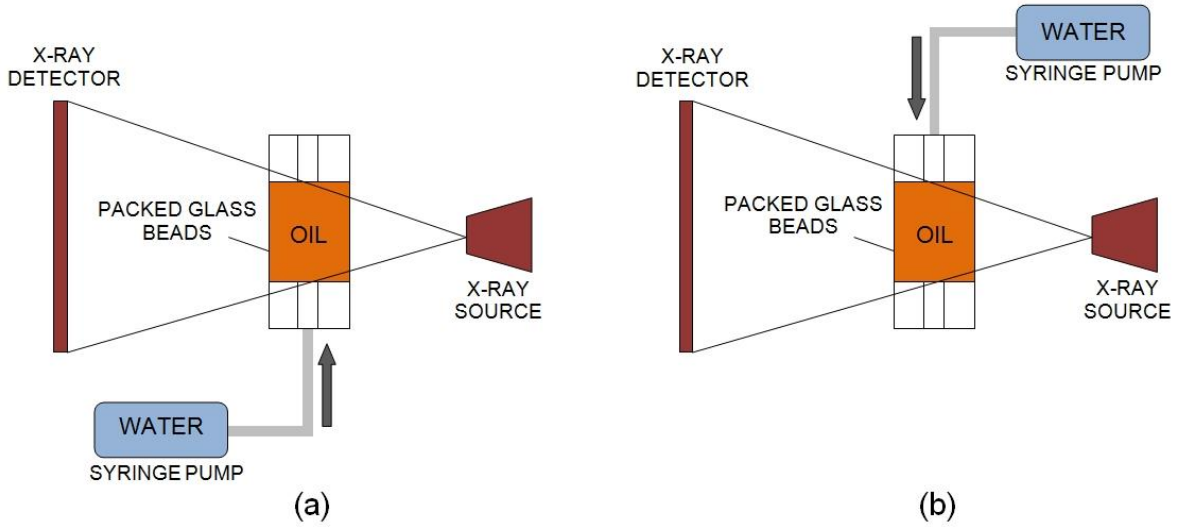

Fig. 2.3 Experimental setup: (a) upward injection (b) downward injection

In this experiment we used pure water as water phase with density 998 kg/m3. For the oil phase, we used dodecane doped with 10% iododecane by weight to increase its X-ray attenuation with combined density 780 kg/m3. For porous media, we utilized water-wet glass beads fabricated using silica fibers, 350 – 500 μm (average 400 μm) in diameter, packed in an acrylic resin tube with an inner diameter and height of 10 mm. We conducted

experiments with variations in upward and downward injections in order to determine the effects of buoyancy forces on the immiscible displacement (Fig. 2.3). The buoyancy forces may have significant effects on the microscopic mechanisms of the displacement in porous media (Morrow and Songkran 1981).

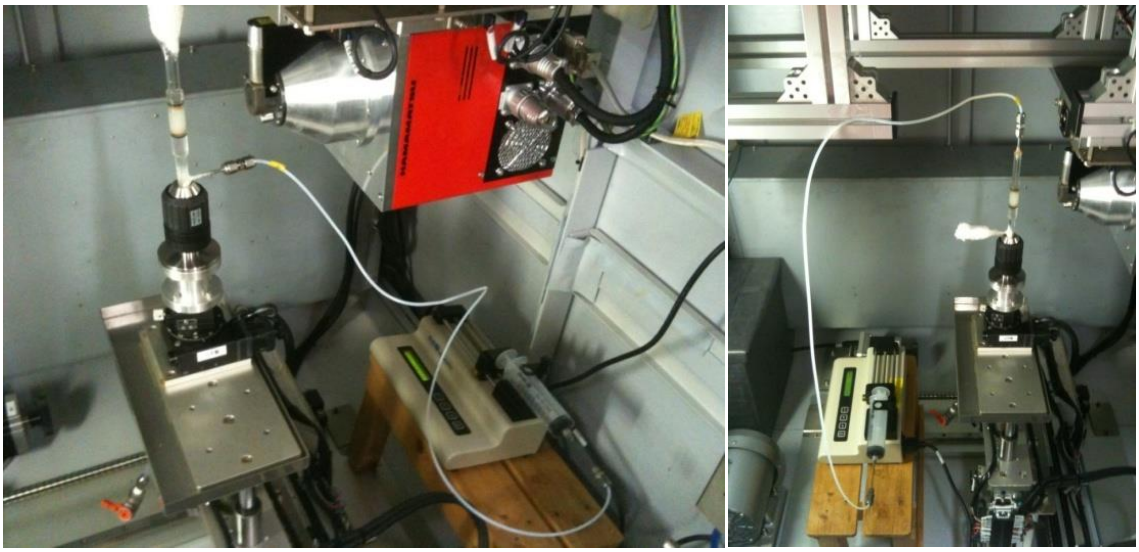

(a) (b)

Fig. 2.4 (a) Experimental setup (upward injection) (b) Experimental setup (downward injection)

We filled the acrylic resin tube with dodecane and added the glass beads slowly in order to avoid air entrapment. For the upward water injection experiment, we continuously injected the water from the bottom of the tube. We scanned every 30 minutes discontinuing when the oil blobs appeared stationary in the X-ray CT monitor indicated that oil blobs were unable to migrate because interfacial tension held them in pore space and they were trapped. For the downward water injection experiment, we repeated the same experimental method except that the water was injected from the top of the tube.

Injections were conducted in two different flow rates. First, we injected upward and downward with injection flow rate 0.06 ml/h resulting water velocity 2.2×10^{-7} m/s. Second, we injected upward and downward with injection flow rate 0.09 ml/h resulting water velocity 3.3×10^{-7} m/s. We varied injection flow rate in order to determine the effect of injection flow rate in pore-scale multiphase phenomena. We studied the imbibition phenomena by using

a low injection flow rate so that the displacement was slow enough to neglect inertial effects. In theory, the imbibition process is determined by the competition between viscous and capillary forces that is represented by the capillary number. In this experiment, the capillary number Ca was defined as the ratio of the viscous force to the capillary force in the pore scale:

$$\mathrm{Ca} = \mu V / \gamma \qquad (2.1)$$

where V is the displacing phase velocity 2.2×10^{-7} m/s and 3.3×10^{-7} m/s, μ is the viscosity of pure water as wetting phase 1.002 mPa·s, and γ is interfacial tension between water and dodecane 51.81 ± 0.09 mN/m (Amaya et al. 2002); therefore, Ca was 4.3×10^{-9} and 6.4×10^{-9}. For additional information, density (ρ) was 998 kg/m^3 for the water phase (pure water) and 746 kg/m^3 for the oil phase (dodecane) and injection flow rate was 0.06 ml/h.

If Ca is lower than 10^{-6}, the trapping mechanism will be dominated by the capillary force, and theoretically, the viscous force can be neglected (Morrow and Songkran 1981). Although we used a pump to inject the pure water, the imbibition process can be considered spontaneous imbibition because the driving force of the process is the capillary force.

Bond number can also be calculated by assuming the system as simple tube (Løvoll et al. 2005). The Bond number was defined as the ratio of the gravitational force to the capillary force in the pore scale:

$$Bo = \frac{\Delta\rho g l \bar{r}}{2\gamma} \qquad (2.2)$$

where l is tube length 10 mm and $\bar{r}$ is the average channel radius . For packed glass beads having diameter 400 – 600 μm (average 500 μm), the average pore throat size is 38.7 μm (Al-Raoush and Wilson 2005). By assuming that the pore throat as the smallest channel with highest threshold capillary pressure, we can get rough estimation of pore throat size for packed glass beads having diameter 400 μm, that is 31 μm. Bond number in this experiment was 3.7×10^{-3}.

2.2.2 Image processing

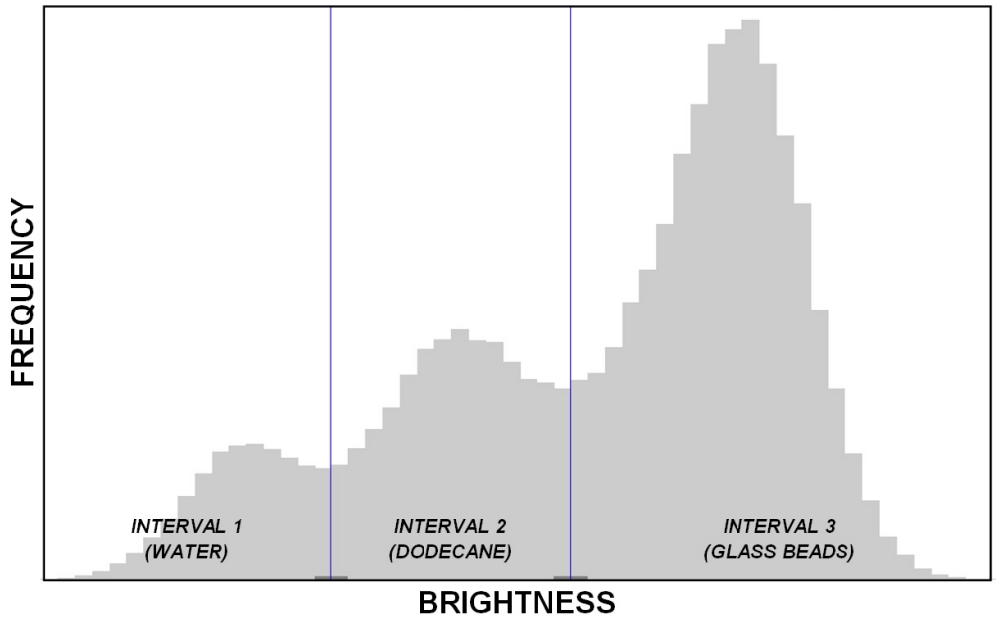

Fig. 2.5 Brightness interval of gray-scale image

In this experiment, the X-ray CT scanner produced gray-scale images with a resolution of 20.799 µm/pixel. Recent development of micro-ct offering high-resolution sensor and high-accuracy image reconstruction software makes us possible to get spatial resolution as high as 1 micron and even better than it. However, high resolution does not mean the best resolution. Because we are dealing with visualization of small object, the most important thing is not setting the resolution to the highest level, but setting the resolution to the best level. The word “best resolution” is the resolution that makes us possible to observe the phenomena clearly and completely. The resolution of X-Ray CT scanner depends on several parameters. Besides sensitivity of the sensor, image resolution also depends on the distance between source, object, and detector. The maximum image resolution produced by our micro-CT equipment is 3.421µm/pixel. However, if we use this resolution to visualize our experiment, the picture produced will only focus on very small part of packed glass beads and we will not be able to understand clearly how imbibition and oil trapping mechanism work. Because of that reason, we reduce the resolution to 20.799 µm/pixel; the best resolution to visualize the whole intended area. We can see the imbibition phenomena clearly and the scope is big enough. We set their scale, boundary, and optimum brightness

by using Image J (Raband 1997-2008; Abramoff et al. 2004), and then saved them as TIFF images. Each phase has a different brightness interval, as shown in Fig. 2.5.

Detection of each phase is based on the brightness threshold value of each image. We did a lot of trials to get the best combination of fluids so that the brightness difference can be observed clearly. Judging from original grey scale image, we can determine the distribution of water by our own eyes. By setting the brightness threshold value of each image, the phase saturation can be determined for each experiment. We employed global thresholding for determining the distribution of each phase. The threshold value was chosen on the basis of the histogram. To simplify image processing, one threshold value was used for all image slices. To minimize phase misidentification due to image noise, we employed a Gaussian blur. Data from Image J was used to construct 3-D images by using VG Studio Max, through which we set the minimum and maximum brightness and changed the color for each phase (blue, orange, and gray regions represent water, oil, and glass beads, respectively). To clearly observe the flow phenomena, we prepared cross-sectional cuts and sometimes removed oil or water phases from the 3-D images. Because we used a low flow rate, the interfaces moved very slowly, thereby reducing blur effects and enabling clear observation of each imbibition step.

2.3 Results and Discussions

During spontaneous imbibition, the water movement was highly affected by the capillary pressure difference existing in a channel arranged in the glass beads and to a lesser extent, by a pore level gravity bias due to a combination of density difference, high mean pore radius and high enough model height. Figure 2.6a shows a 3-D image of the packed glass beads during the upward water injection.

When two immiscible fluids contact a solid surface, a pressure difference is created and can be expressed as

$$p_c = p_{nw} - p_w = 2\gamma \cos\theta / r \qquad (2.3)$$

where p_{nw} and p_w are pressure in the non wetting phase and wetting phase, respectively; θ is the contact angle; and r is the mean of the radius curvature. In the case of upward injection, pressure acting on the non wetting phase at the interface was higher than that on the wetting phase (Fig. 2.6b). However, at the start of upward imbibition, the non wetting phase remained in a continuous phase relative to atmospheric pressure; therefore, the

pressure gradually reduced toward the outlet. On the other hand, the wetting phase pressure at the bottom of the tube was higher than that at the interface because the wetting phase was connected to a syringe pump. The pressure gradient in the wetting phase and non wetting phase caused both phases to spontaneously move upward.

In downward injection experiment, pressure distribution caused by interaction between wetting phase and non wetting phase along injection direction is same with upward injection experiment. At the interface, the pressure acting on the wetting phase was lower than that on the non wetting phase (Fig. 2.7b). The wetting phase pressure increased toward the inlet at the top of the tube because it was connected to a syringe pump. On the other hand, the non wetting phase pressure decreased toward the outlet at the bottom of the tube connected to atmospheric pressure. The pressure gradient caused the wetting phase and non wetting phase to spontaneously move downward, and this capillary pressure gradient in upward and downward injections initiated imbibition. This mechanism is known as the initiation of imbibition.

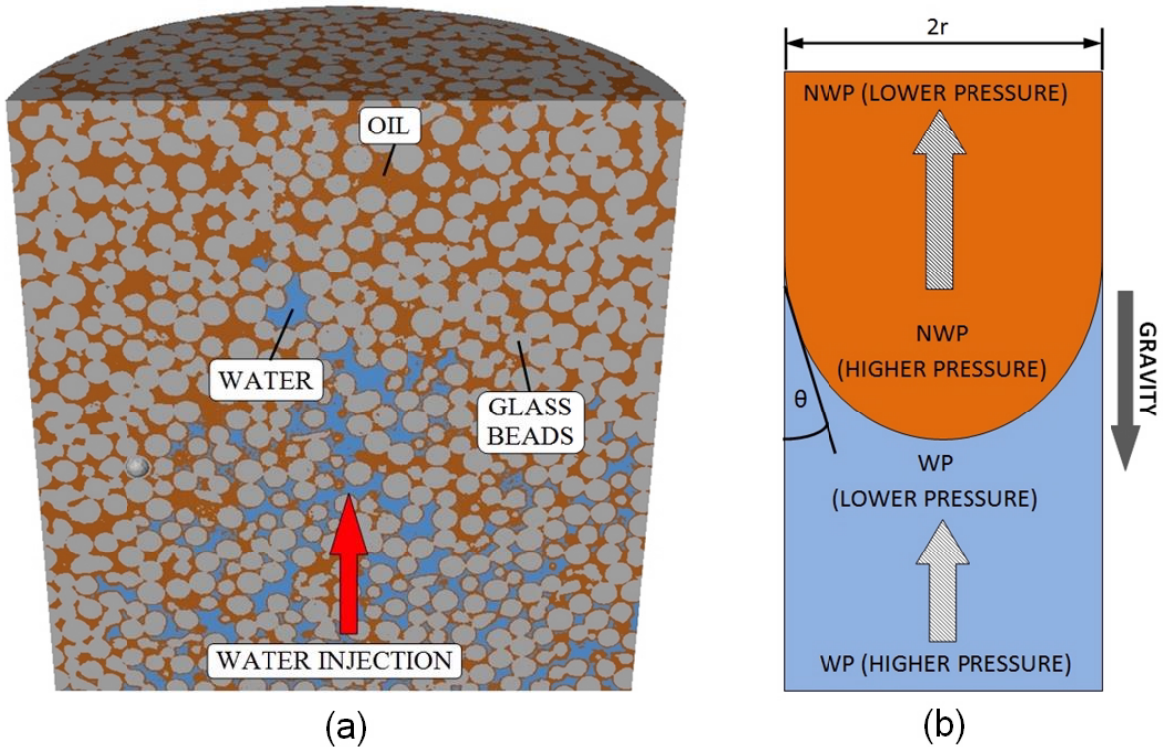

Fig. 2.6 (a) 3-D cross-sectional view of packed glass beads (b) initiation of imbibition process in upward injection

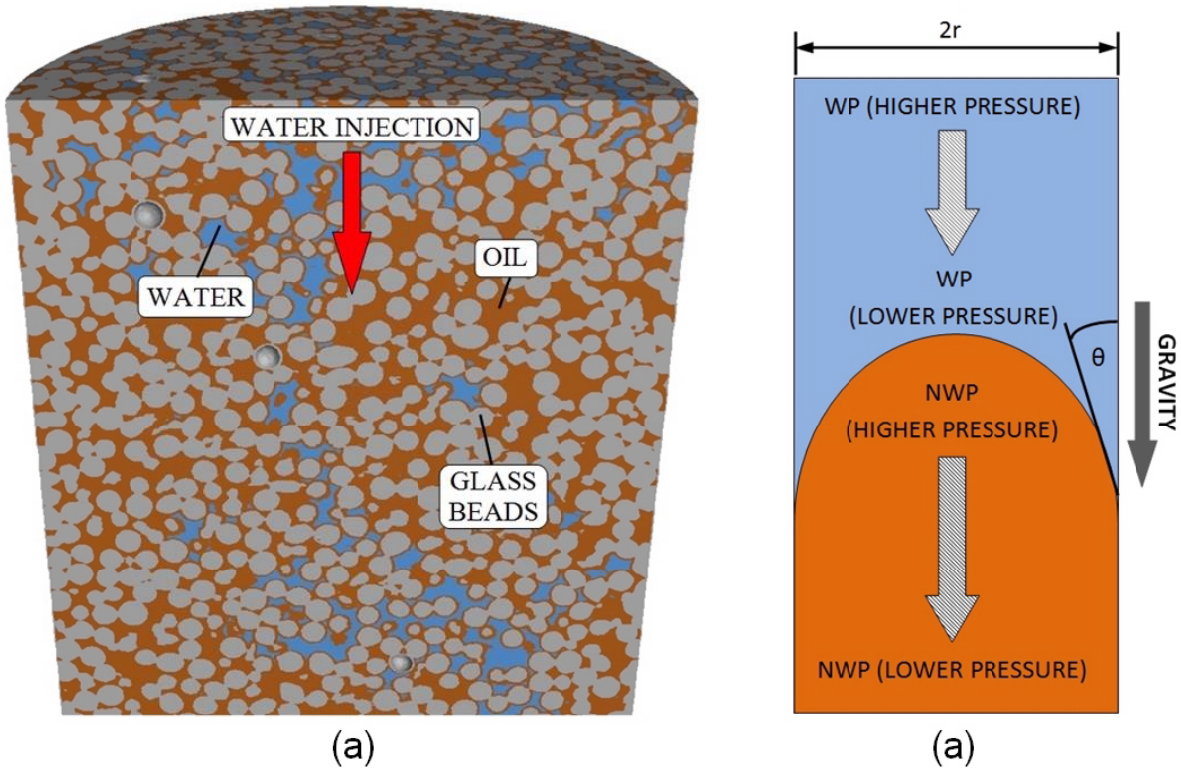

Fig. 2.7 (a) 3-D cross-sectional view of packed glass beads (b) initiation of imbibition process in downward injection

2.3.1 Properties Change During Imbibition

The final oil saturation in the upward water injection was approximately 30% for capillary number 4.3×10^{-9} and 6.4×10^{-9} (Fig. 2.8 and Fig. 2.9). The interesting point here is that the final oil saturation along the 10 mm tube length was nearly constant. This is because in the upward water injection, the interface movement is sufficiently stable, resulting in high and uniform sweep efficiency.

The characteristic saturation profile of the downward injection as shown in Fig. 2.10 and Fig. 2.11 is different from that of the upward injection shon in Fig. 2.8 and Fig. 2.9. The final saturation at each point was distributed non-uniformly along the tube. The main reason for this phenomena is that in the downward oil injection, fingering phenomena occurred severely. Therefore, oil blobs of various sizes were trapped, leading to fluctuation in the final saturation. Because fingering phenomena dominated the imbibition process, the final saturation of each position varied depending on its pore configuration.

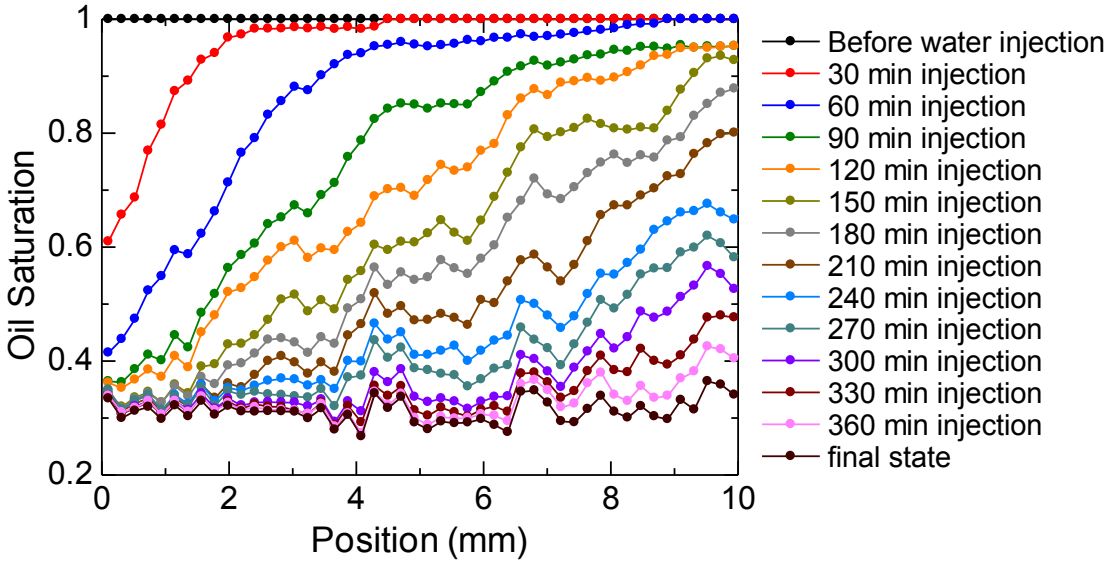

Fig. 2.8 Oil saturation change in upward injection Ca = 4.3×10^{-9}

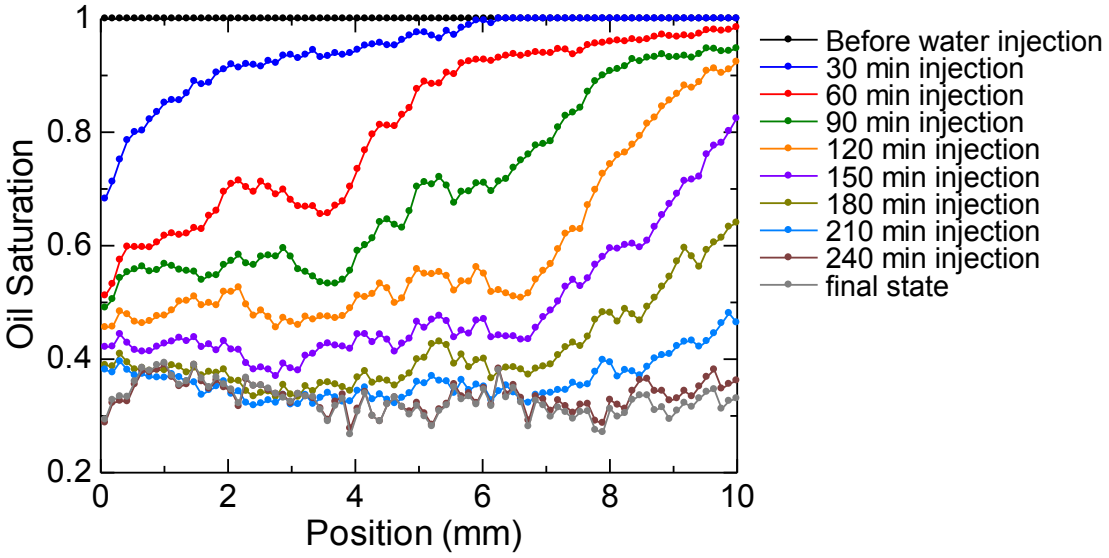

Fig. 2.9 Oil saturation change in upward injection Ca = 6.4×10^{-9}

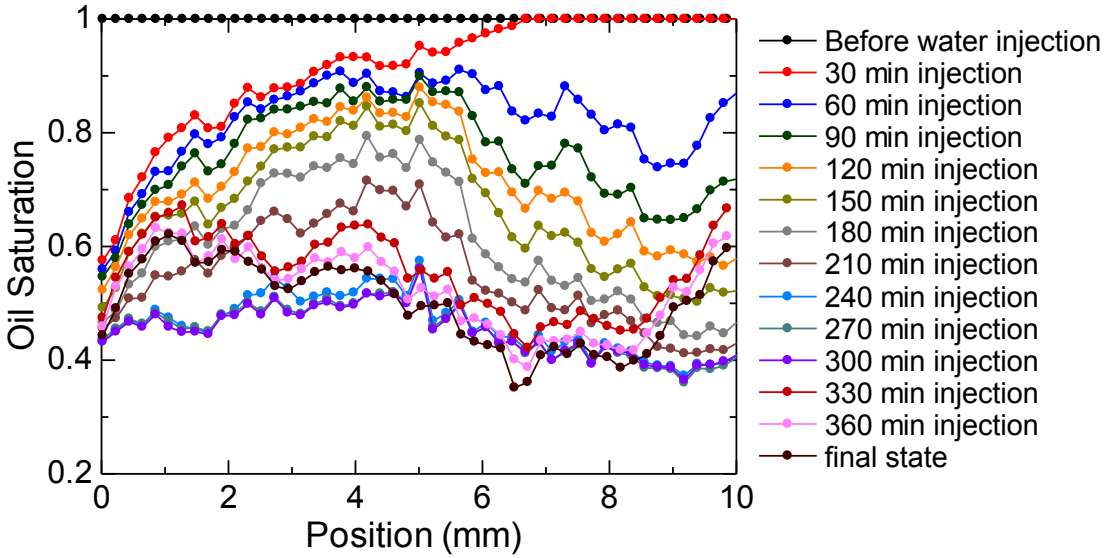

Fig. 2.10 Oil saturation change in downward injection Ca = 4.3 × 10^{-9}

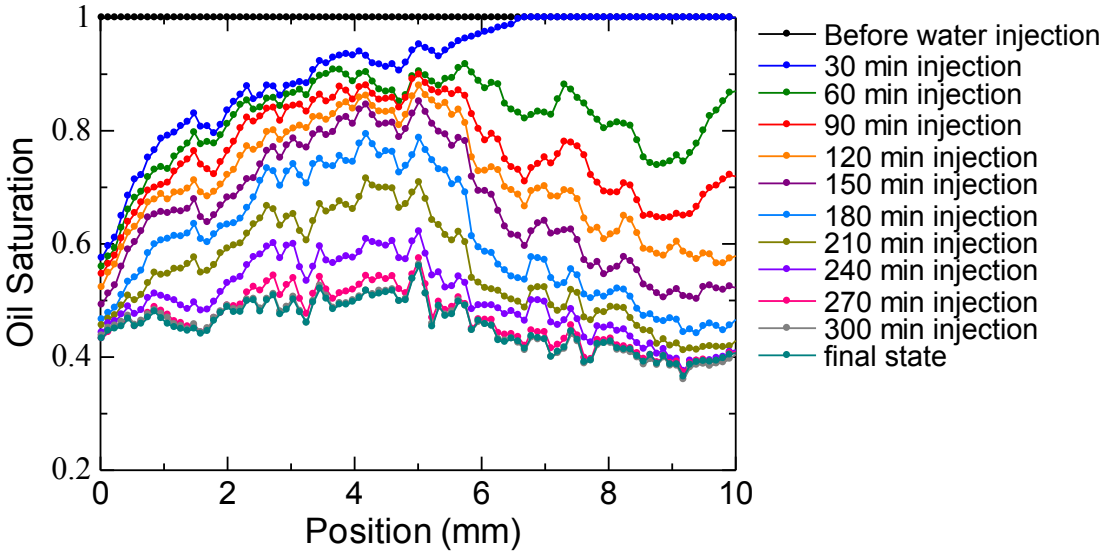

Fig. 2.11 Oil saturation change in downward injection Ca = 6.4 × 10^{-9}

To calculate the local velocity of oil, we applied the material balance approach (Goodfield et al. 2001), which can be expressed as

$$U_{oil}(z,t) = U(t)F_{oil}^{inj}(t) - \frac{\partial V_{oil}(z,t)}{\partial t} \qquad (2.4)$$

where $U_{oil}(z,t)$ is the local velocity of oil in z position and at time t, $U(t)$ is the total fluid injection velocity in the inlet, and $F_{oil}^{inj}(t)$ is the fraction of oil in the inlet at time t. Oil volume per unit cross-sectional area between the packed glass beads and position z, $V_{oil}(z,t)$, is defined by

$$V_{oil}(z,t) = \int_0^z \phi(\zeta) S_{oil}(\zeta,t) d\zeta \qquad (2.5)$$

Here, $\phi(\zeta)$ is the porosity of the porous media in specific positions and $S_{oil}(\zeta,t)$ is the oil saturation in specific positions and at time t. Thus, the local velocity of oil at time t in specific positions can be summarized as follows:

$$U_{oil}(z,t) = \frac{V_{oil}(z,t) - V_{oil}(z,t+\Delta t)}{\Delta t} \qquad (2.6)$$

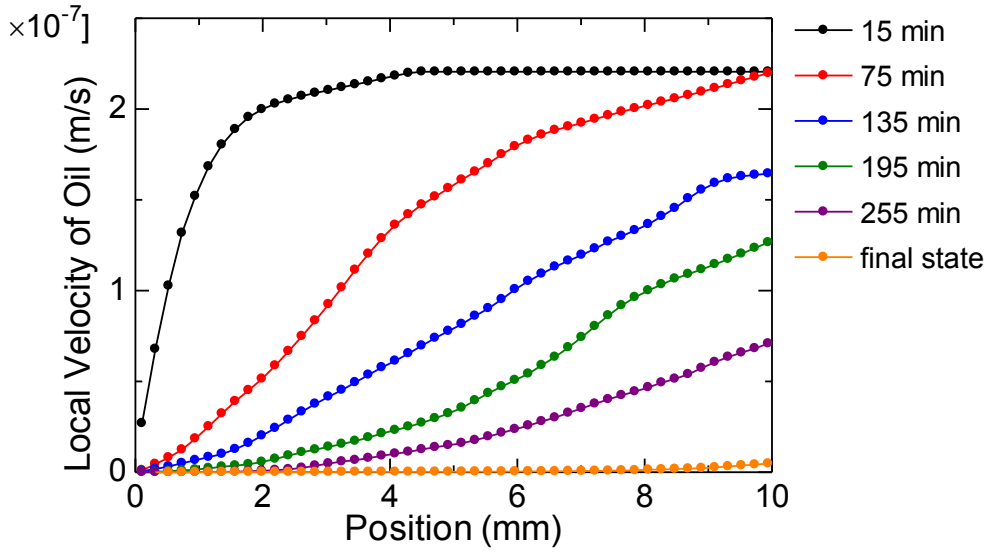

Fig. 2.12 Oil velocity change in upward injection Ca = 4.3 × 10^{-9}

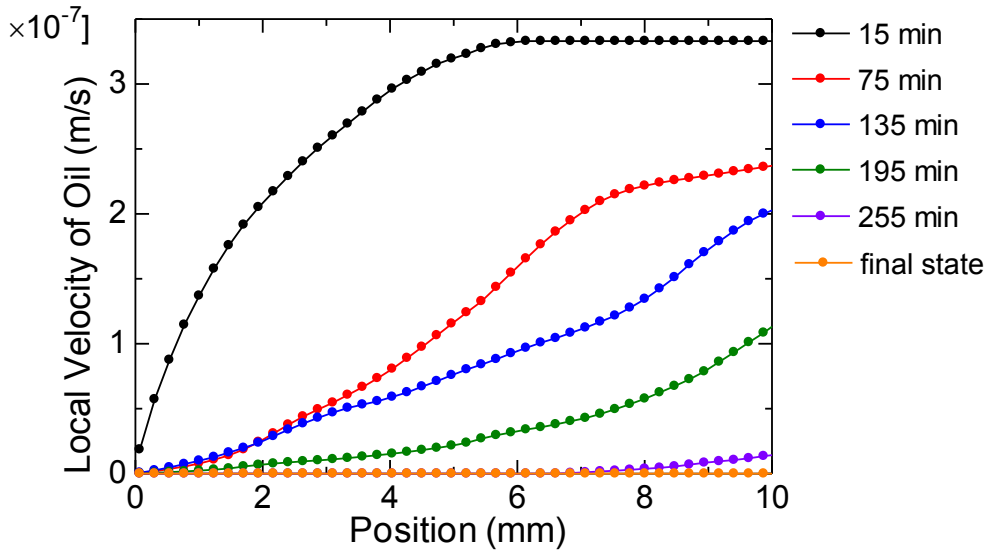

Fig. 2.13 Oil velocity change in upward injection Ca = 6.4 × 10^{-9}

The local velocity of oil can be calculated from the saturation data by using Eq. 2.6. An oil velocity of 0 m/s indicates that oil has already been trapped. In the upward water injection, the local velocity of oil gradually reduces as water invades the pore space (Fig. 2.12 and Fig. 2.13); this is due to the steady interface movement in the upward injection experiment.

In the downward water injection, it is obvious that the local velocity of oil reduces dramatically after water invasion (Fig. 2.14 and Fig. 2.15). This is because in the downward water injection, the fingering phenomena occurs severely, causing low sweep efficiency; that is, the water prefers to penetrate channels previously invaded during the fingering phenomena. Hence, only oil contained in the invaded channels migrate and the rest remain in its original position. If the water path connecting inlet and outlet has been completed, the remaining water will easily flow through that path and only a part of the water will flow through another path.

Water will only flow through another channel if a pore space that is more favorable than the path previously created exists (pores with smaller diameters than that of adjacent water paths). Therefore, after the water fingers are created, only a part of the oil is extracted. As a result, first the local velocity of oil reduces significantly, and then reduces gradually because of the fingers' radial growth.

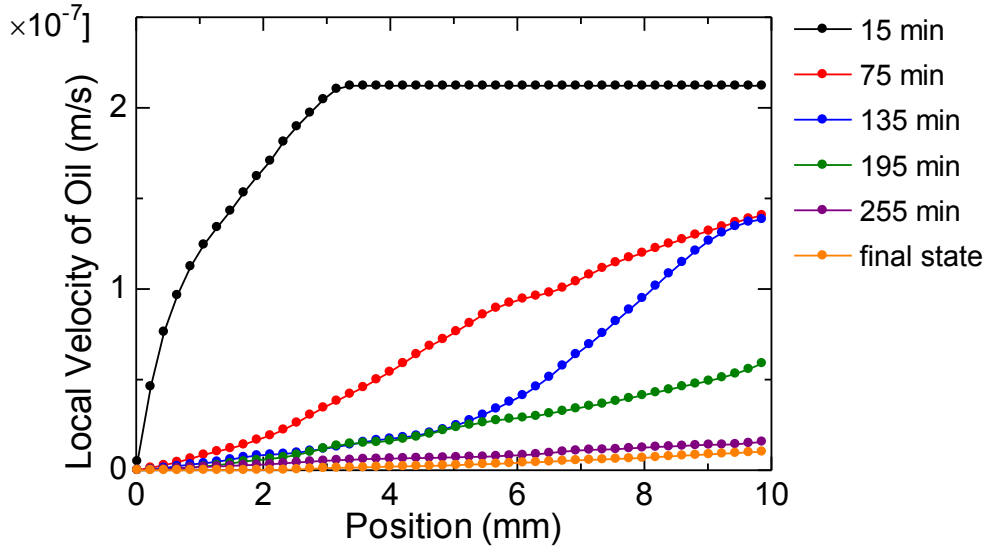

Fig. 2.14 Oil velocity change in downward injection Ca = 4.3 × 10^{-9}

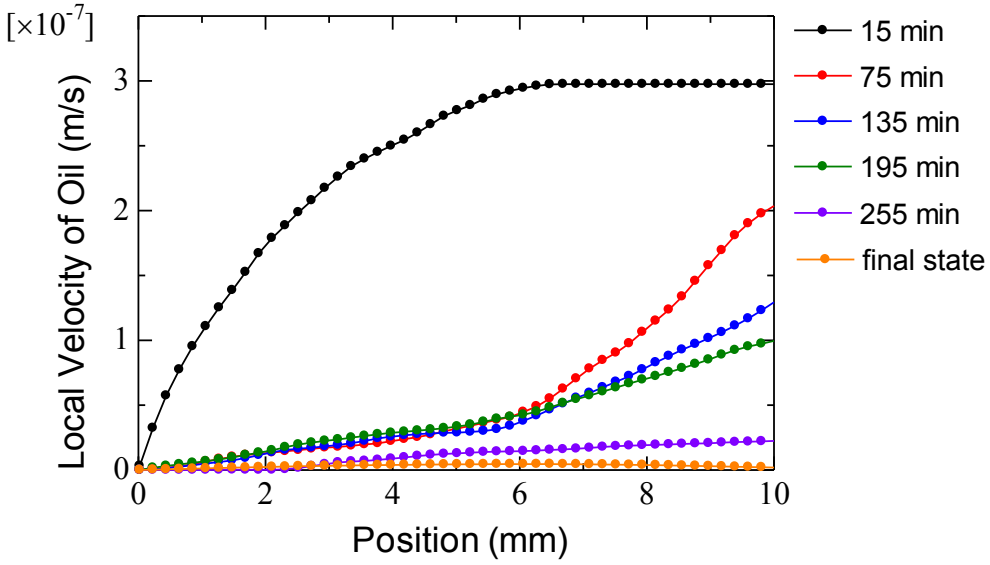

Fig. 2.15 Local velocity of oil during downward WP injection Ca = 6.4 × 10^{-9}

2.3.2 Fingering Phenomena

Water and dodecane viscosity are 1.002 mPa·s and 1.344 mPa·s at 20 ˚C, respectively. Because the water viscosity is lower than that of dodecane, interface instability occurs when the wetting phase displaces the pore filled by the non wetting phase (Saffman 1958).

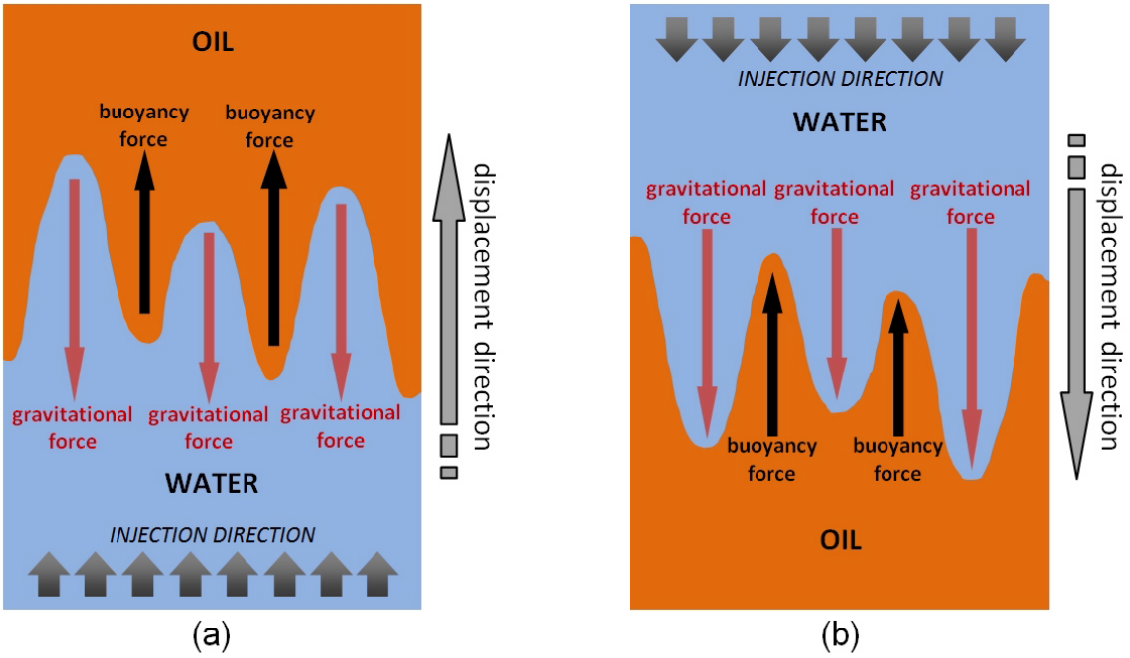

Fig. 2.16 Interface stability: (a) upward injection (b) downward injection

In spontaneous imbibition, the wetting phase moves faster in smaller channels because its capillary pressure is higher. Differences in imbibition rates in each channel also initiate the fingering phenomena. Due to fingering, the wetting phase sweeps only part of the porous medium, leading to a breakthrough and inefficient oil recovery (Lenormand 1989). Fingering is affected by many variables such as viscosity differences between the wetting phase and non wetting phase, capillarity, gravity, and the pore structure.

Figure 2.16 shows the interface stability in upward and downward injections. In the upward injection, the gravitational force acts as a stabilizer (Fig. 2.16a). At the interface, the buoyancy force tends to move oil upward and the gravitational force suspends the water movement because its direction is different from that of the water injection; therefore, finger

growth can be reduced. In the downward injection, as shown in Fig. 2.16b, the gravitational force acts as the initiating force for finger growth because its direction is the same as that of the injection. At the interface, the buoyancy force also supports the finger growth and can be significant, especially at low flow rates or high density ratios. By comparing the results of the upward and downward injections, we can observe the influence of gravity on spontaneous imbibition.

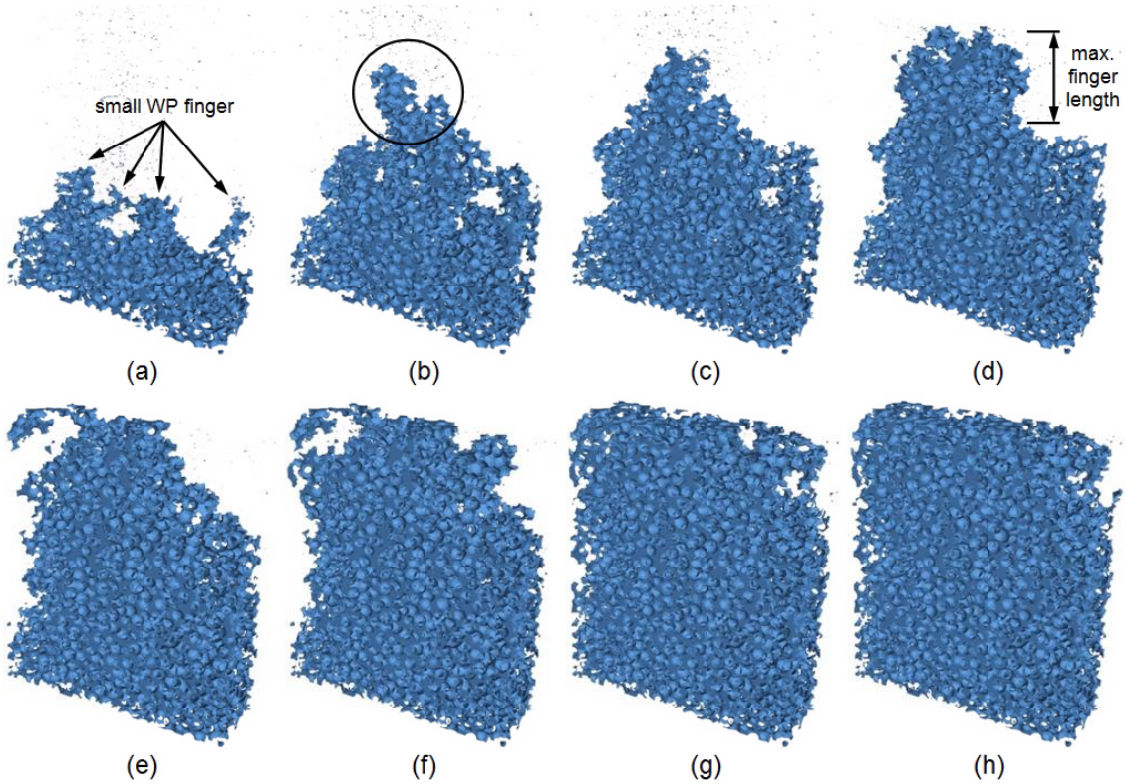

Fig. 2.17 Water movement during upward injection Ca = 4.3×10^{-9}: (a) 30 minutes (b) 60 minutes (c) 90 minutes (d) 120 minutes (e) 150 minutes (f) 180 minutes (g) 210 minutes (h) steady state

Three dimensional pictures showing figering phenomena in upward and downward WP injection were made by digitally removing glass beads and oil. We set the thickness at the middle of the tube to approximately 2 mm because it will show water fingers clearly and reduce overlapping by other water fingers. Figure 2.17 shows the water movement in the upward injection with capillary number 4.3×10^{-9}. At the beginning of the imbibition process, because there was no considerable external force acting on the system, water movement was dependent on the capillary pressure attracting it. Grain configurations that created

various sizes of channels with different capillary pressures tend to initiate the occurrence of small water fingers (Fig. 2.17a). However, these fingers could not grow because gravity stabilized their movement, (Fig. 2.16a). During imbibition, small fingers are stabilized, allowing the remaining larger fingers to grow (Fig. 2.17b). However, the water fingers also could not expand and had the tendency to grow radially instead of lengthwise. From Figs. 2.17a and 2.17b, it is obvious that the finger growth was controlled by the capillary pressure differences in each channel and the effect of the competition between the gravitational and buoyancy forces, which resulted in a relatively stable displacement. Gravity has a more significant effect on longer fingers measured in the vertical direction. Therefore, the fingers can grow up to a maximum length before capillary differences compete against gravity, causing the fingers to grow radially.

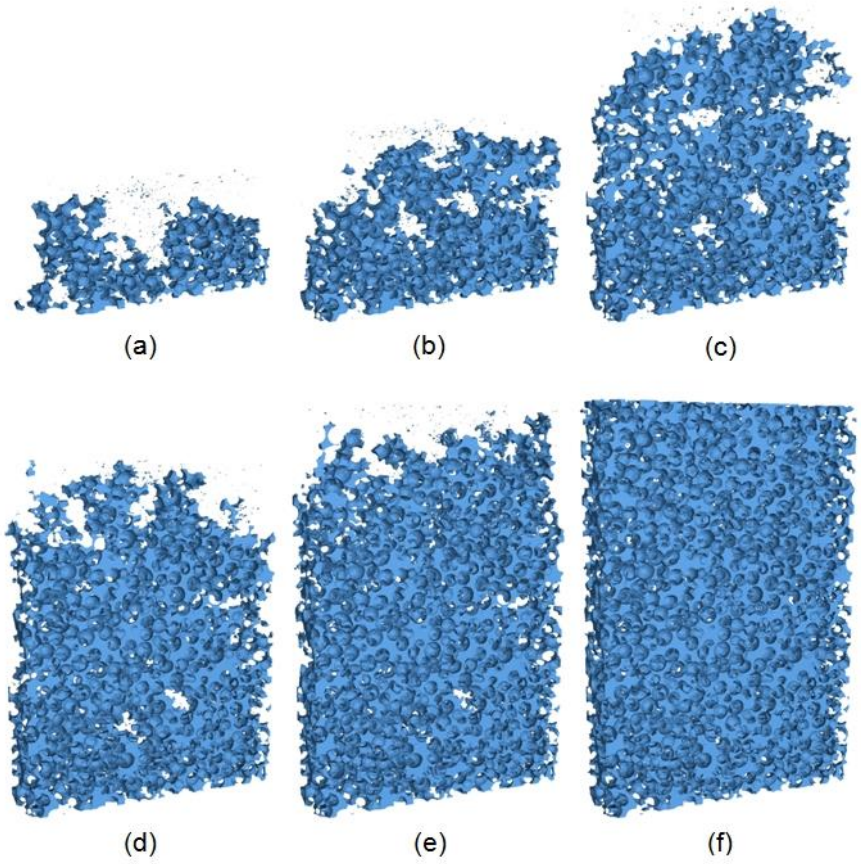

Fig. 2.18 Water movement during upward injection Ca = 6.4×10^{-9}: (a) 30 minutes (b) 60 minutes (c) 90 minutes (d) 120 minutes (e) 150 minutes (f) steady state

Figure 2.18 shows the water movement in the upward injection with capillary number 6.4×10^{-9}. At the beginning of the imbibition process, because there was no considerable external force acting on the system, water movement was dependent on the capillary pressure attracting it. Grain configurations that created various sizes of channels with different capillary pressures tend to initiate the occurrence of small water fingers (Fig. 21a). However, because of interaction between bouyancy and gravitational force tends to stabilize water fingering phenomena, small figers seen in Fig. 2.18a was disappeared in Fig. 2.18b and stable displacement was achieved. From Figs. 2.17c–2.17f, it is obvious that the displacement process in upward injection was very stable. This result confirmed previous result (capillary number 4.3×10^{-9}) and proved that during upward water injection, water finger was stabilized.

In 3-D porous media and the upward water injection, the bouyancy and gravitational forces maintain the displacement constant, leading to high sweep efficiency. However, the channel diameter differences in porous media must be considered. In this experiment, we used glass beads with an approximate diameter of 400 μm. Even water channels created from almost uniform grain configurations have different sizes. Therefore, small fingering due to the capillary pressure differences in each channel resulted in different imbibition speeds.

Figure 2.19 illustrates the fingering phenomena in the downward injection with capillary number 4.3×10^{-9}. In the downward injection, the gravitational and bouyancy forces initiated the finger growth. Water prefers to flow in smaller pores; in Fig. 2.19b, the water appears to selectively determine the most suitable flow path toward the outlet. The direction of the finger growth was affected by the pore configuration. In Fig. 2.19c, water has reached the outlet. It is clear that the water only flowed in the left part of the image, which shows non-uniformity of the water movement due to the fingering phenomena. Figures 2.19d–2.19h illustrate the water finger growth in the radial direction.

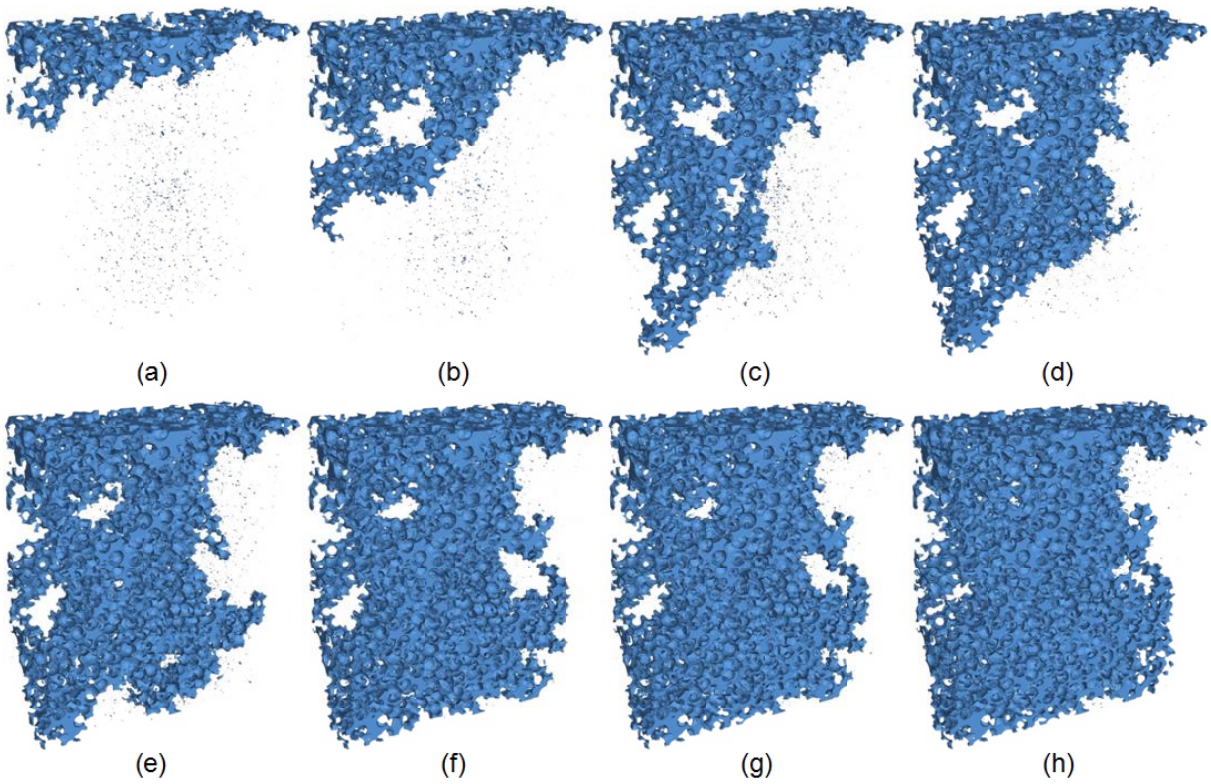

Fig. 2.19 Water movement during downward injection Ca = 4.3 × 10^{-9}: (a) 30 minutes (b) 60 minutes (c) 90 minutes (d) 120 minutes (e) 150 minutes (f) 180 minutes (g) 210 minutes (h) steady state

Figure 2.20 shows the fingering phenomena in the downward injection with capillary number 6.4 × 10^{-9}. The phenomena is almost same with Fig. 2.19. In the beginning of imbibition, water appears to selectively determine the most suitable flow path toward the outlet and small water finger was created as we can see in Fig.2.20a. Once that water path was created, water tends to flow only through it causing finger growth. Water will only flow through surrounding channels if those channels have higher capillary pressure and the direction is affected by the pore configuration. From Fig. 2.20b we can see that water finger in the middle part spread into many channels at the lower part of tube, leaving big oil blob in the middle part. Figures 2.20c–2.20f illustrates the water finger growth in the radial direction. After the water paths from the inlet to the outlet were completed, water not only flowed through that path but also resulted in radial growth of fingers, increasing sweep efficiency. The capillary pressure in the pores surrounding the fingers attracted the water, causing it to flow through the pores. Figure 2.19 and 2.20 shows that after the water path from the inlet

to the outlet was completed, water not only flowed through that path but also resulted in radial growth of fingers, increasing sweep efficiency. This means that the capillary pressure in the pores surrounding the fingers attracted the water, causing it to flow through the pores while the capillary pressure was sufficiently strong for water to invade the pore space.

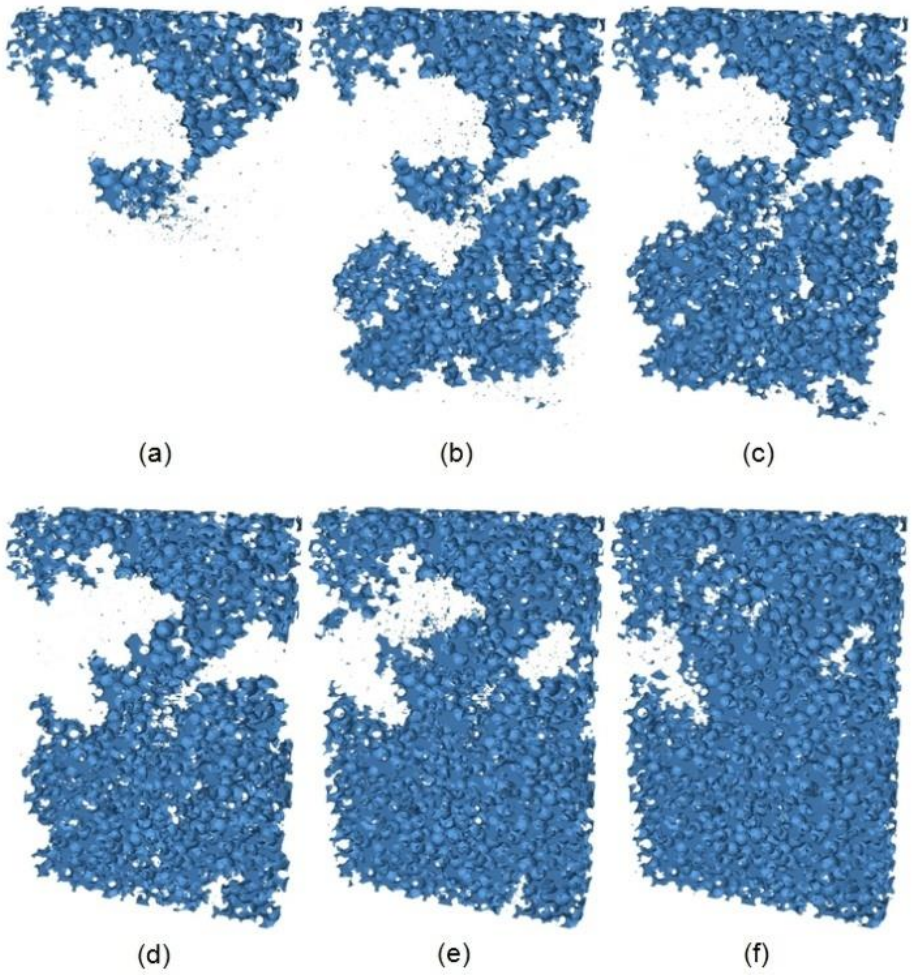

Fig. 2.20 Water movement during downward injection Ca = 6.4×10^{-9}: (a) 30 minutes (b) 60 minutes (c) 90 minutes (d) 120 minutes (e) 150 minutes (f) steady state

Selective water movements in porous media during the downward water injection tend to disrupt the oil continuity, reducing the oil production efficiency. The imbibition path is driven by capillary pressure and the stability is determined by the competition between the buoyancy and gravitational forces. Oil recovery was higher during upward injection because the water invades pore space almost uniformly. In this experiment, the imbibition speed was

so small that even in 10 mm long sample, fingering grew dramatically. Bond number in this experiment was 3.7×10^{-3}. Because Bond number represents comparison between hydrostatic pressure to the capillary pressure, it means that capillary pressure in our experiment is far bigger than pressure gradient due to buoyancy. However, by comparing Figs. 2.17, 2.18, 2.19, and 2.20, it is obvious that the water movement varies during upward and downward injections proving that the buoyancy effect was big enough.

2.3.3 Oil Trapping Mechanism

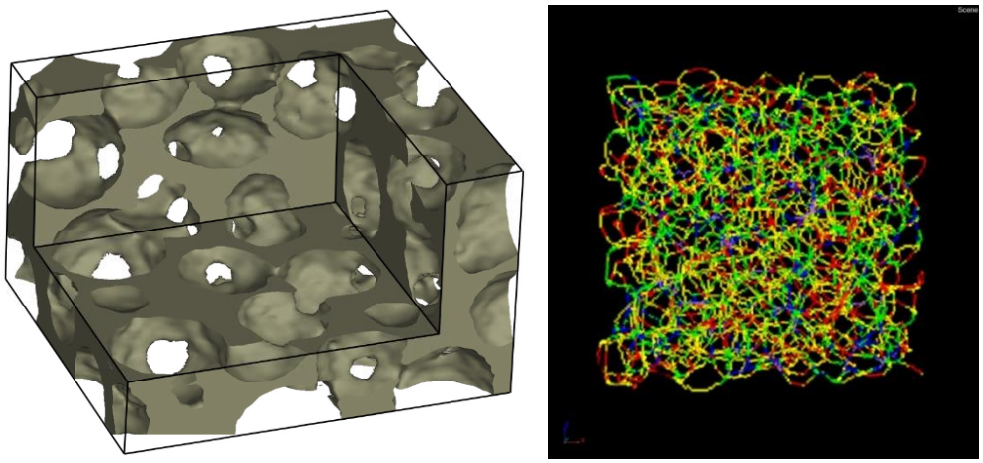

(a) (b)

Fig. 2.21 Complex and heterogeneous channels in porous medium (a) reconstructed image of small cluster pores (b) Medial axes on grain with diameter and height of 10mm

Because the pore structure is complex, observing an actual 3-D trapping mechanism is difficult, especially when the focus is a pore-scale event. Grain configurations create complex and heterogeneous web-like channels (Fig.2.21).

Fig. 2.22 illustrates the trapping phenomena in the upward injection with capillary number 4.3×10^{-9}; water is represented as a transparent form. At the beginning of imbibition, WP tends to flow in a smaller channel with a higher capillary pressure difference. Figure 2.22b illustrates that the grain configuration drives the WP movement. During the invasion, because of the different imbibition speeds in each channel and the influence of pore geometry, there is a possibility that the water movement in one channel can disrupt the NWP continuity (Fig. 2.22c). It is obvious that during the initial trapping process, the NWP continuity is always disrupted by the dominant water movement process. In Fig. 2.22d, it

appears that in several pores, a part of the oil is isolated by water. However, the possibility remains that some pores are still connected with those surrounding them. Thus, a part of the oil can escape and the remaining is trapped (Fig. 2.22f).

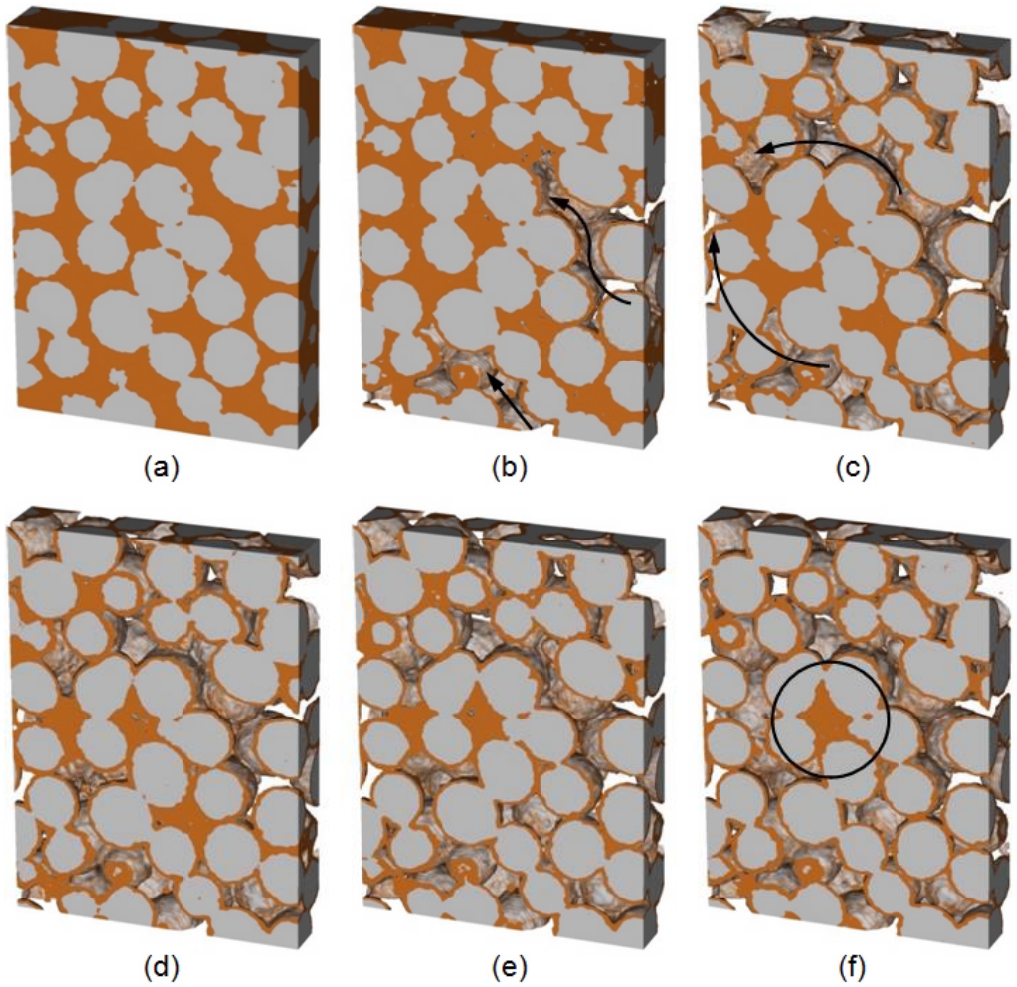

Fig. 2.22 Nonwetting phase trapping process in upward injection Ca = 4.3 × 10^{-9} oil saturation: (a) before wetting phase invasion (b) 30 minutes later (c) 60 minutes later (d) 90 minutes later (e) 120 minutes later (f) steady state

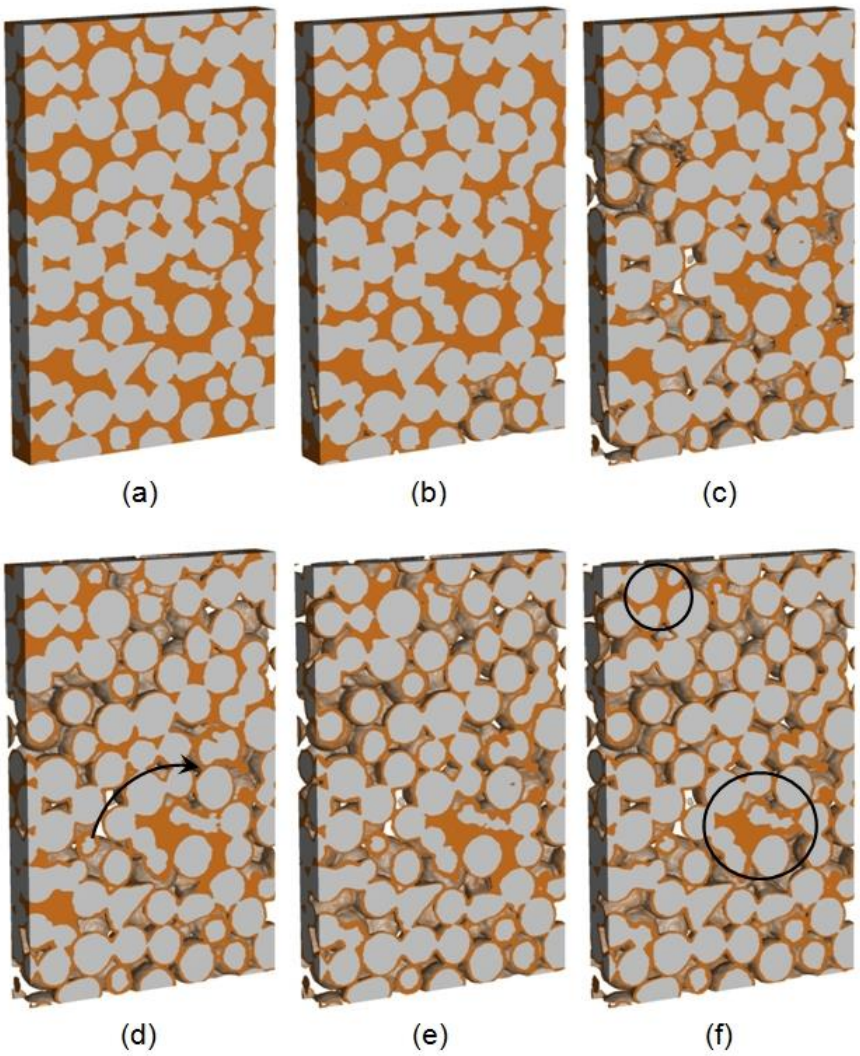

Fig. 2.23 Nonwetting phase trapping process in upward injection Ca = 6.4×10^{-9} : (a) before water invasion (b) 30 minutes (c) 60 minutes (d) 90 minutes (e) 120 minutes (f) steady state

Figure 2.23 illustrates upward injection experiment with capillary number 6.4×10^{-9}; water is represented as a transparent form. The phenomena was almost same with Fig. 2.23. At the beginning. Water movement will be affected by pore geometry. Figure 2.23c illustrates that the grain configuration drives the water movement. Imbibition speed different in each channel creates heterogeneity of oil-sweeping process. Because of it, there is a possibility that the water movement in one channel can disrupt the oil continuity as shown in Fig. 2.23d. It is obvious that during the initial trapping process, the oil continuity is always disrupted by

the dominant water movement process. In Fig. 2.23e, it appears that in several pores, a part of the oil is isolated by water. A part of the oil can escape and the remaining is trapped (Fig. 2.23f). The most important fact in Fig.2.23 is that in upward water injection, oil is likely trapped because of imbibition speed different in each channel disrupting oil continuity and oil is trapped in single or small cluster of pores.

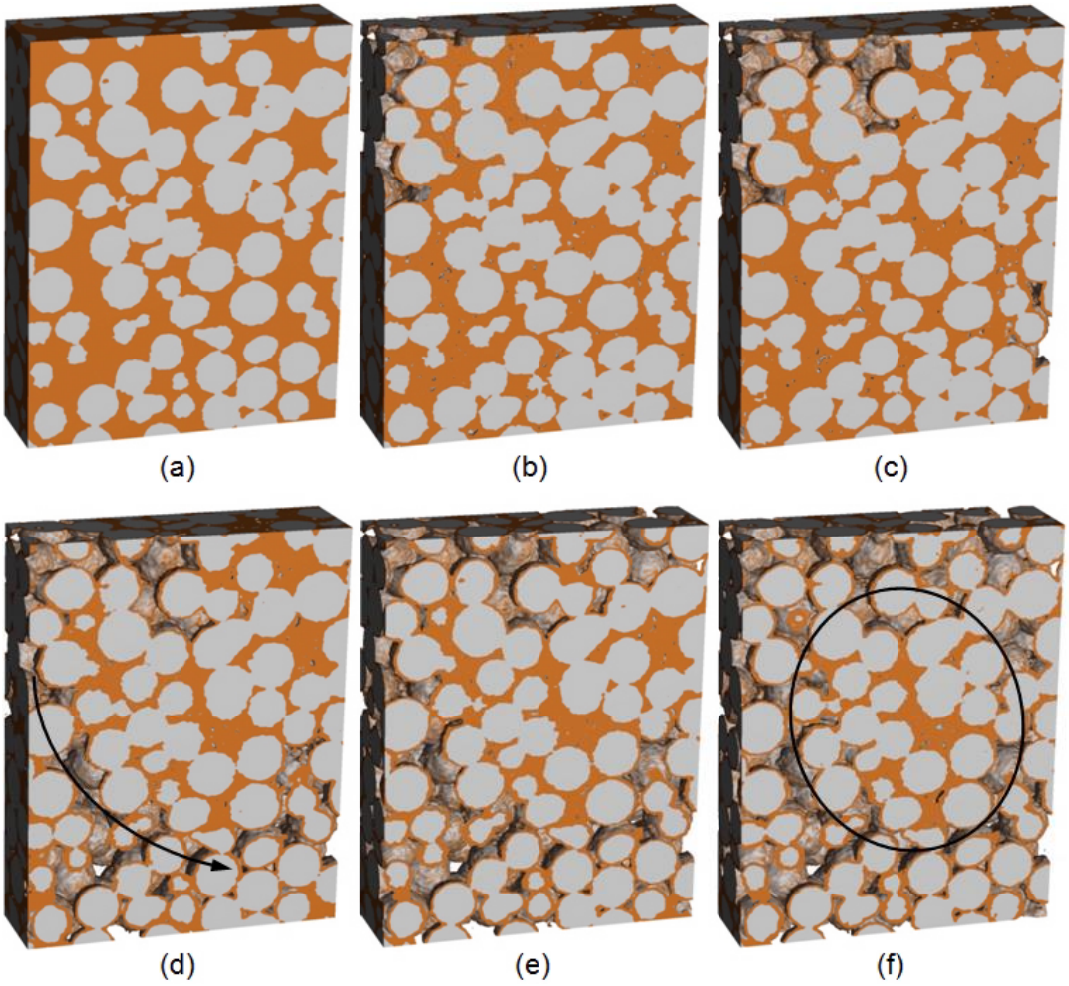

Fig. 2.24 Nonwetting phase trapping process in downward injection Ca = 4.3 × 10^{-9} oil saturation: (a) before wetting phase invasion (b) 30 minutes later (c) 60 minutes later (d) 90 minutes later (e) 120 minutes later (f) steady state

The trapping process in the downward injection was nearly the same as that in the upward injection except that fingering plays a dominant role. At the beginning of imbibition, water invades pore space with higher capillary pressure. The competing capillary pressures

of the surrounding pores in the radial direction (perpendicular to tube axis) and axial directions (parallel to tube axis) during fingering growth cause water to unevenly invade pore space. If the capillary pressure in the surrounding pores in the axial direction is stronger, water tends to move in that direction, causing longer water fingers. The most important event in this image occurs when the water movement disrupts the oil continuity and causes oil blob entrapment in several pore spaces (Fig. 2.24d). Water invasion is unevenly distributed, leaving large oil blobs in the pore-space clusters. The size of the oil blob in the downward water injection is much larger than that of the upward water injection. This is because long water fingers occurring in the downward water injection cause large oil blobs to be skipped and trapped. The competing buoyancy and gravitational forces at the interface in the downward water injection accelerate the finger growth, as shown in Fig. 2.16b. The distance between each finger causes water to only sweep a part of the porous medium; thus, once water disrupts the continuity of an oil blob, it is trapped in pore-space clusters.

At the beginning of imbibition, water flew in a smaller channel with a higher capillary pressure difference as shown in Fig. 2.25b. In Fig. 2.25c, we can see that water flowing from other channels overtook large oil blob located in the middle of tube. At this time, oil was still in the continuous form. Fig. 2.25d – Fig. 2.25f show the trapping mechanism of large oil blob. After overtaking the oil blob, water continuously invaded pores around it causing discontinuity of oil. At this time, water was capable of doing overtaking-like movement because gravitational and buoyancy force supported water finger growth and did not stabilized the interface. The most important event in this image occurs when the water movement disrupts the oil continuity and causes large oil blob entrapment (Fig. 2.25f). The size of the oil blob in the downward water injection is much larger than that of the upward WP injection because long water fingers occurring in the downward WP injection cause large oil blobs to be skipped and trapped. The competing bouyancy and gravitational forces at the interface accelerate the finger growth. The distance between each finger causes water to only sweep a part of the porous medium. Once water disrupts the continuity of an oil blob, it is trapped in pore-space clusters.

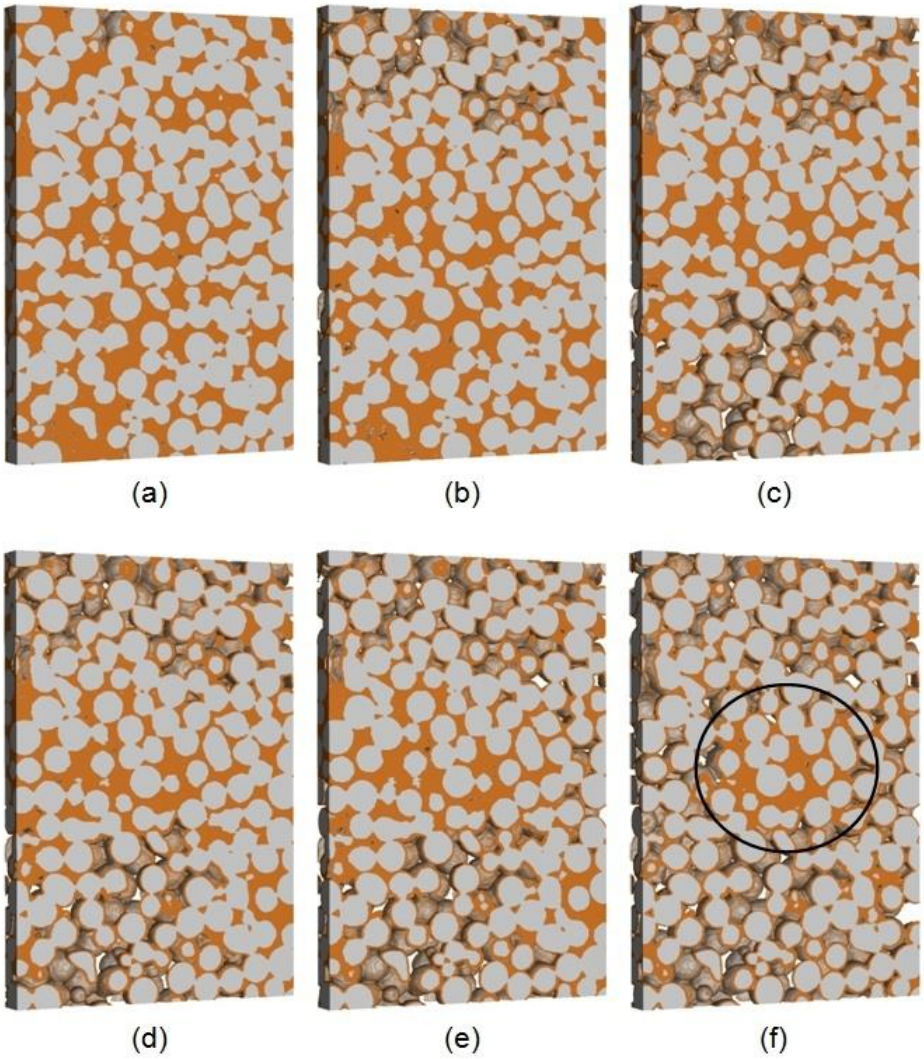

Fig. 2.25 Nonwetting phase trapping process in downward injection Ca = 6.4×10^{-9} : (a) before water invasion (b) 30 minutes (c) 60 minutes (d) 90 minutes (e) 120 minutes (f) steady state

2.4 Conclusions

The trapping mechanism in the upward and downward water injections is nearly the same and is dominated by the imbibition speed differences in some channels. Imbibition speed different caused by variation of channel size disrupted oil continuity and it is trapped inside pore space because interfacial tension prevent its migration. Oil is trapped not only in single pores but also in pore-space clusters. Cluster trapping is possible if the configuration

meets the trapping criteria. Because the interface moves steadily in the upward injection, only small water fingering occurs, resulting in small oil blobs size. In downward imbibition, because fingering occurs severely, the finger size determines the trapped oil amount, and oil is trapped in pore-space clusters (network scale) rather than in single pores. In this study, snap-off mechanism was not a dominant factor for oil trapping process.

3 THREE-DIMENSIONAL IMAGING OF PORE-SCALE WATER FLOODING PHENOMENA IN WATER-WET AND OIL-WET POROUS MEDIA

3.1 Background

Water flooding is one of the most important processes in oil production. Water is injected into an oil reservoir to maintain the reservoir pressure, and the water sweeps some of the oil toward the production well. During this process, some oil is left behind by the water and becomes trapped in the porous reservoir medium. The stability of the displacement front of the water is highly affected by variations in the pore channel diameters, which cause capillary pressure differences and capillary fingering, thus reducing the sweeping efficiency. The differences in density and viscosity between the displacing and displaced fluids enhance the instability of the displacement front (Cinar et al. 2009). Usually, less than 50% of the original oil in a reservoir can be recovered using water flooding, the rest becoming trapped because of the capillary pressure holding it in the pore spaces. Understanding the phenomena inside the reservoir rock by direct observations is a crucial step toward developing an advanced water flooding method that will significantly improve the oil recovery factor.

So far, many studies of the water flooding process have been conducted using micromodels etched on a glass plate (Chang et al. 2009; Jamaloei et al. 2010) or simulations (Blunt et al. 1992). Micromodels usually describe the water flooding process in two dimensions, and water flooding simulations require many parameters to be precisely determined. An additional scheme is required for the process to be studied more realistically. Pore-scale observations in 3D porous media offer a solution, because pore-scale processes govern the fundamental behaviors of the multiphase flow phenomena in porous media (Al-Raoush and Wilson 2005). The development of microfocused X-ray computed tomography (CT) scanner technology now allows the nondestructive visualization of the phenomena (Kumar et al. 2010), and its application allows observations that are critical to our understanding of fluid transport.

Water flooding in natural or artificial porous media has been observed using microfocused X-ray CT scanners, yielding parameters such as saturation, flow distribution, trapped oil size, and trapped oil distribution can be observed. Water flooding phenomena

have been observed over time in many studies. Usually, only the initial state (before water is injected) and the final state (after water has been injected) are observed, and the resolution and image quality limit observations to, at best, a cluster of pores. Moreover, the effect of wettability difference in pore scale has not been clearly observed three dimensionally. In previous chapter, water invasion process and oil trapping mechanism were observed only in only water-wet porous medium. Moreover, there were some graphical error caused by X-ray broadening effect. In this chapter, more comprehensive observation were conducted not only in water-wet porous medium, but also in oil-wet porous medium. Observation methods were also improved in order to produce more detail and precise images. Variation of wettability in actual porous medium may cause some variation in water flooding behavior.

In this paper, the water flooding processes in water-wet and oil-wet porous media were visualized over time by using a microfocused X-ray CT scanner. A scheme was developed so that allows the time-dependent processes, including the initial state, the initiation of water invasion, the invasion pattern, and the trapping phenomena, can be observed clearly, step-by-step. These phenomena can be visualized in 3D in a single pore and in a cluster of pores.

3.2 Experiments

3.2.1 Experimental Scheme

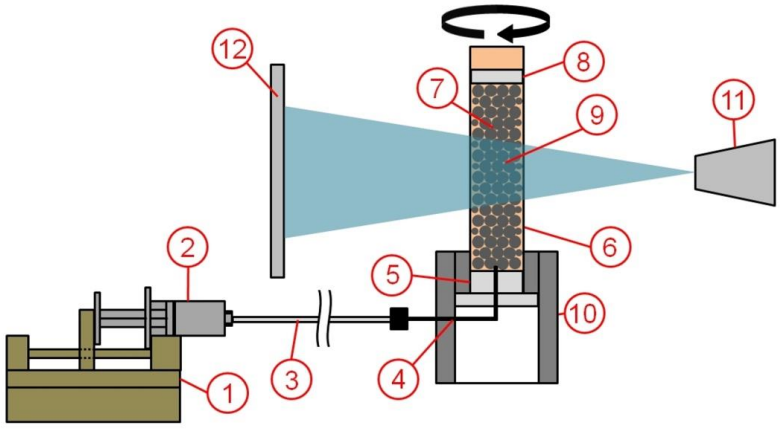

Fig. 3.1 Experimental setup. (1) Syringe pump, (2) syringe, (3) tubing, (4) needle, (5) bottom cap, (6) resin tube, (7) glass beads, (8) filter, (9) observed area, (10) holder, (11) X-ray source, (12) X-ray detector.

The water flooding process was visualized using a microfocused X-ray CT scanner (ScanXmate-G100S110; Comscantechno Co.). The image resolution depended on the ratio of the distances between the X-ray source, detector, and the object. The focal spot size of the X-ray CT scanner used in this experiment was 5 μm. The X-ray CT scanner captured 600 projections from angular orientations while the object is spinning 360 degrees during its process. The commercial software embedded with the X-ray machine reconstructed the most probable image in equally spaced grid size that consist of 512 images showing cross sectional view along the porous medium. The resolution of those 512 images was 504 × 504 pixels.

The X-ray CT scanner produced images in gray scales, whose intensity was proportional to X-ray absorption. Iodododecane doped with 23 wt% dodecane was used as the oil phase and distilled water as the water phase, to allow the phases to be distinguished clearly in the images. The properties of each phase used are listed in Table 1. Two different glass bead treatments were used. Glass beads fabricated from silica fibers, with diameters of 350–500 μm (average 400 μm), were used as oil-wet glass beads. In addition, the same glass beads washed with toluene, ethanol, and then water, to remove the coating, were used as water-wet glass beads.

A tube with an inner diameter of 4 mm and height of 50 mm was filled with oil, and the glass beads were poured slowly into it, avoiding entrapping air. The packed glass beads were scanned to determine the initial conditions. Water was then injected upward at Ca = 4.9×10^{-7} for 2 hours. The experimental setup is shown schematically in Fig. 3.1. The capillary number, Ca, is defined as the ratio of the viscous force to the capillary force at the pore scale (equation 3.1).

$$\mathrm{Ca} = \mu V / \gamma \qquad (3.1)$$

where V is the displacing phase velocity, μ is the water viscosity, and γ is the interfacial tension between the oil and water. The displacing phase velocity was adjusted to 1.1×10^{-5} m/s. The interfacial tension between water phase and oil phase was 22.5 mN/m measured by the pendant drop method. At capillary numbers below 10^{-6}, the trapping mechanism will be dominated by capillary forces, and the viscous force can be neglected (Morrow and Songkran 1981).

To observe critical phenomena during water invasion and oil trapping process, porous medium was scanned every minute for the first 30 minutes. Finally, steady state

condition was scanned after injection of water for 2 hours. Each scanning process took 60 seconds with 10 frames per second. By using such a scheme, the water invasion process can be visualized clearly.

Table 3.1. Properties of fluids

Fluids	Composition	Density, g/cm^3	Viscosity, mPa·s
Water	Distilled water	0.998[a]	1.002[b]
Oil	Iodododecane 77 wt% + dodecane 23 wt%	1.068[a]	3.110[c]

[a]Measured at 20ºC

[b]Measured by Kestin *et al.* (Kestin et al. 1978)

[c]Measured with falling ball viscometer at 20ºC

3.2.2 Image Processing

The image resolution was 9.484 μm/pixel, and the scale, boundary, and optimum brightness were set using the image processing software ImageJ (Abramoff et al. 2004). To allow the system to be visualized clearly, the tube was set as close as possible to the X-ray source. A 4 mm high section of the tube, approximately in the middle of the tube, was observed so that the entrance and exit effects were excluded.

Each phase was visualized with a different brightness, as shown in Fig. 3.2. The glass beads, water, and oil were distinguished using appropriate brightness threshold values for each phase and they could be independently removed, digitally, from each 3D structure at each time interval, if required. We used global thresholding, choosing the threshold values from the histogram. Change of the brightness threshold value for 1 or 2 points above or below the correct value may cause less than 1% difference in water and oil saturation.

Images from the image processing software were used to construct 3D images using the volume rendering software VG Studio Max 2.1. Images at the initial conditions were used to construct the glass bead structures for all data. The volume fraction and position of glass beads structure were checked in each time interval to confirm that it remained in the same position. Images from each time interval were used to digitally extract the water phase and oil phase independently. The 3D glass bead image under the initial conditions was then

combined with the 3D water phase and 3D oil phase images to create a complete structure at each time interval.

The iododododecane and dodecane mixtures (oil phase) and pure water (water phase) were carefully selected with two aims: to limit the buoyancy effect between the oil and water phases and to achieve an oil phase brightness that left the glass bead brightness between the oil and water brightnesses. A major consideration was the X-ray broadening effect. The brightness should change step-wise at the interface between two substances with different X-ray absorption coefficients. However, in images, the interface is broadened, creating a slope-like shape, decreasing the accuracy with which the boundary can be located, especially when phenomena in a single pore space are being observed. If the phase brightnesses are in the order water, oil, then glass beads, from low to high, the broadening of the interface between the water and glass beads creates the illusion of an oil film on the surface of the glass beads. To eliminate this, each image set should have a reference image subtracted, in order to digitally separate the oil and water phases. However, this takes time and leads to another error that is caused by the improper subtraction process, because of irregularities in the image sets.

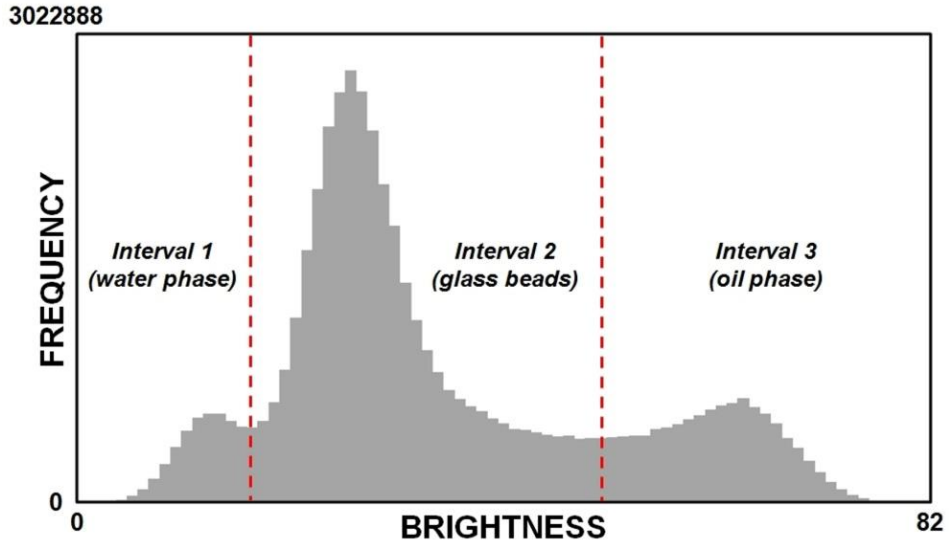

Fig. 3.2 Brightness intervals in the gray-scale images.

3.3 Results and Discussion

Two types of displacement processes commonly occur when one fluid is displaced by another immiscible fluid in a porous medium. The first most common process is piston-like displacement, where the displacing fluid invades the pore space filled with the displaced fluid with a movement that is similar to that of a piston. During drainage, the nonwetting fluid enters pores filled with the wetting phase only if the capillary pressure is equal to or greater than the threshold capillary pressure. The second process is snap-off, which only occurs when the wetting phase in a pore throat occupied by the nonwetting phase collapses and cuts off the continuity of the nonwetting phase.

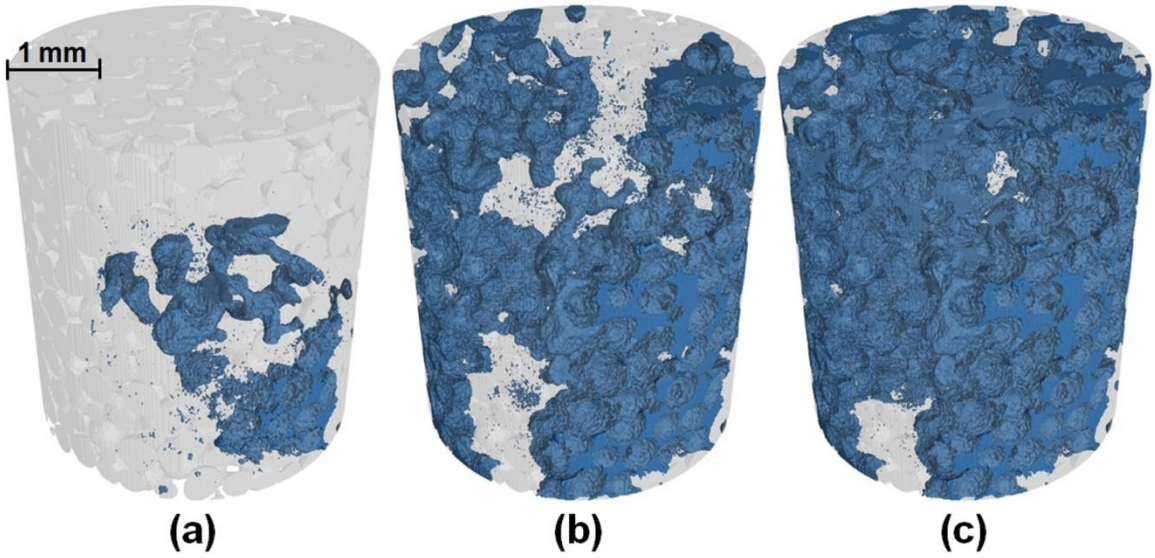

Fig. 3.3 Water flooding process in oil-wet glass beads. (a) 1 minute, (b) 5 minutes, and (c) 2 hours after water injection was started. Blue regions indicate water.

Figure 3.3 shows the water flooding process in oil-wet glass beads. The real-time observations of the pore-scale phenomena were clearly observed in this system. Because the porous medium was oil-wetted, the nonwetting water phase drained the wetting oil phase. The water tended to invade the larger pores because of the lower capillary pressure threshold. Therefore, at the early stage of drainage shown in Fig. 3.3a, the water had invaded the pores close to the wall, which are more porous because of the sorting effect. Different invasion speeds in each channel caused oil entrapment, as shown in Fig. 3.3c. In

the water-wet porous medium, the water tended to spontaneously invade channels with a high capillary force.

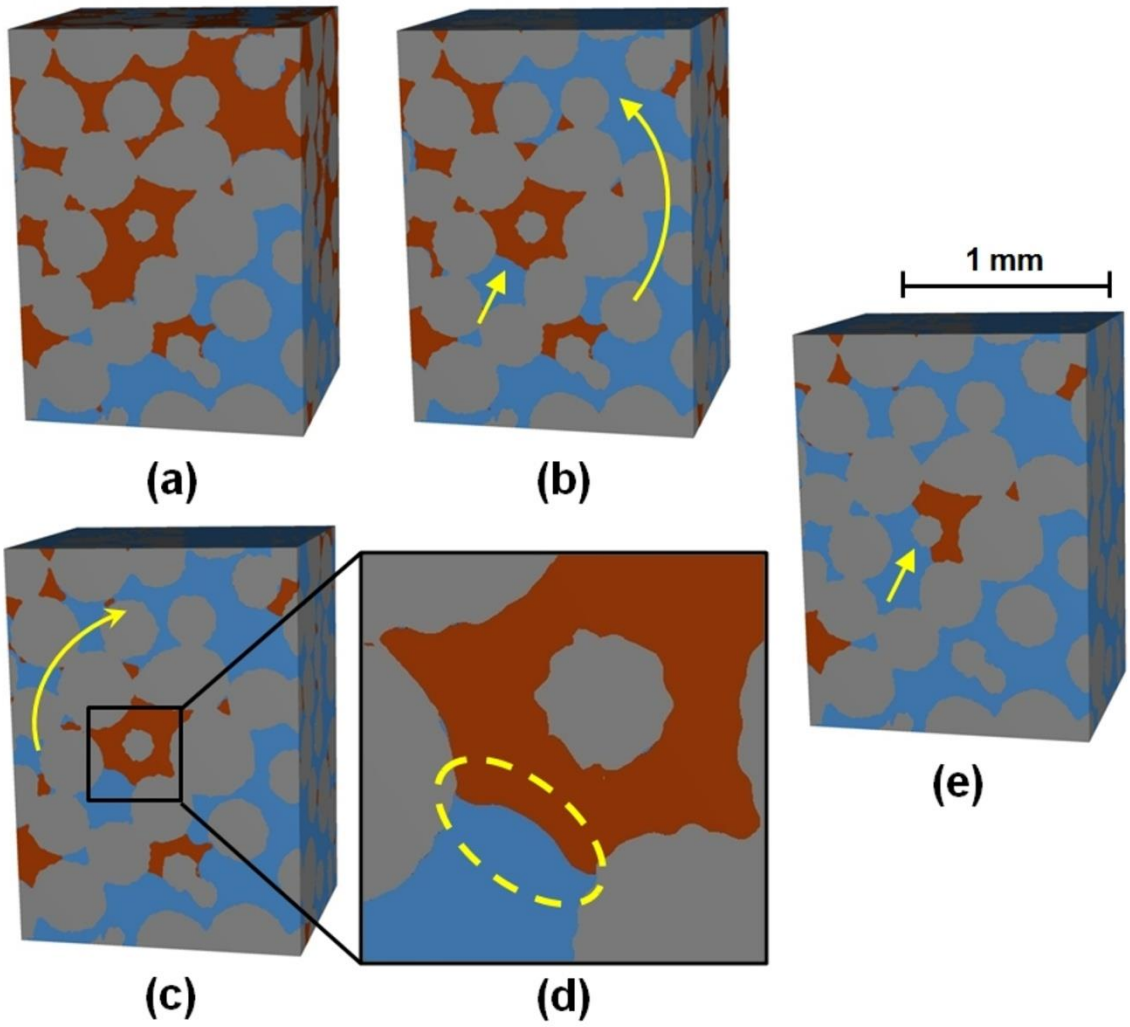

Fig. 3.4 Observed pores in an oil-wet porous medium. (a) Water injection for 1 minute, (b) water injection for 2 minutes, (c) water injection for 3 minutes, (d) shape of the interface, (e) water injection for 2 hours. Orange, blue, and gray regions indicate oil, water, and glass beads, respectively.

The water invasion pattern can also be observed by magnifying the packed glass beads, as shown in Fig. 3.4. In the oil-wet porous medium, the water tended to invade pores with larger channel diameters, as shown in Fig. 3.4a. The displacement front was not

homogeneous because of channel diameter variability. The yellow lines in Fig. 3.4b shows instability of the displacement front. Some of channels containing oil were more preverable to be invaded by water than others. In Fig.3.4c, the yellow line shows how the invasion of water from another side of observed pore happened, creating overtaking-like manuever and cutting continuity of the oil. This process is a major mechanism in oil trapping process (Blunt and Scher 1995). Because of the overtaking-like maneuver, oil blobs are discontinued and trapped as shown in Fig. 3.4e and capillary pressure holds them in the pore spaces.

The yellow arrows in Fig. 3.4b and 3.4e shows how the oil in the pore space was displaced in a piston-like movement. The threshold pressure for piston-like displacement (p_p) can be expressed as

$$p_p = \frac{2\gamma \cos\theta}{r} \qquad (3.2)$$

where γ is the interfacial tension between the oil and water, θ is the contact angle, and *r* is the pore or throat radius (Blunt and Scher 1995). By using volume rendering software VG Studio Max 2.1, 3D images can be rotated freely and appropriate cross section of the selected pore throats can be found. Throat radius and contact angle can be measured directly. Yellow cirlce in Fig. 3.4d shows the shape of the interface between water and oil in a pore throat. From that figure, the throat radius was found to be 0.093 mm, and the contact angle was 69.4°. The threshold pressure for piston-like displacement was approximately 170.21 Pa.

The pore-scale phenomena within a pore space are illustrated in Fig. 3.5. In Fig. 3.5a, the yellow circle shows the snap-off displacement process, which occurs when the wetting phase invades the wall because the wettable pore is occupied by a nonwetting phase, breaking the continuity of the nonwetting phase at the throat. Figure 3.5a shows the exact moment when the snap-off occurs. Instability occurs when the nonwetting oil phase is no longer in contact with the throat wall. The water film gets thicker and the continuity of oil is broken suddenly. Blunt and Scher (Blunt and Scher 1995) also observed that the threshold pressure for snap-off (p_s) can be expressed as

$$p_s = \frac{\gamma(\cos\theta - \sin\theta)}{r} \qquad (3.3)$$

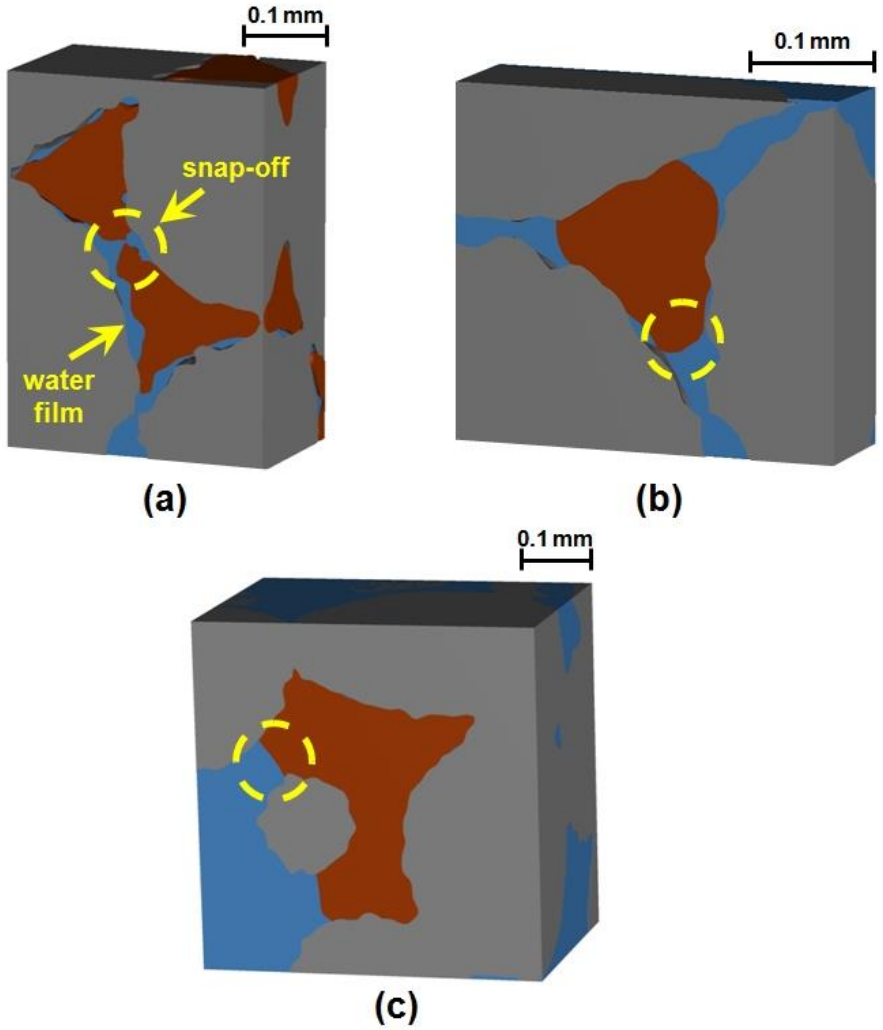

Fig. 3.5 Pore-scale phenomena. (a) Snap-off in a water-wet porous medium, (b) trapped oil in a water-wet porous medium, (c) trapped oil in an oil-wet porous medium. Orange, blue, and gray regions indicate oil, water, and glass beads, respectively.

The throat radius and contact angle could be measured directly from Fig. 3.5a, the throat radius being 0.025 mm and the contact angle 39.6°. Therefore, snap-off occurred at a capillary pressure of approximately 120.04 Pa. Because the threshold pressure for piston-like displacement is always higher than that for snap-off, snap-off occurs only when piston-like displacement is not possible for topological reasons (Fenwick and Blunt 1998). Deriving this parameter from direct observations will allow us to develop water flooding schemes that avoid snap-off as much as possible, resulting in higher oil recovery factors.

Trapped oil in water-wet and oil-wet porous media are shown in Fig. 3.5b and 3.5c. The shape of trapped oil was visualized in a single pore space. In the water-wet porous medium shown in Fig. 3.5b, the trapped oil was convex as shown by the yellow circle, meaning that the water, as the wetting phase, was actually assisted by the capillary pressure to displace the oil from the pore space. However, because the oil had already become discontinuous, the water from any pore throat connected to that pore space acted in the same way, so the water from all of the throats pushed the oil toward the center of the pore space, implying that the oil could not go anywhere else. In the oil-wet porous medium shown in Fig. 3.5c, the trapped oil was concave as shown by the yellow circle. The capillary force in each pore throat would resist water entering the pore space, so the oil would be unable to be displaced simply because water was unable to invade the pore space. The curvature can be seen very clearly, so further improvements in our experimental scheme will allow the capillary pressure holding the trapped oil in place to be calculated from the curvature radius measurement. We could also use the same method in the actual reservoir rock to analyze the wettability of the sample by measuring the contact angle, allowing the prediction of the capillary pressure acting on it during water flooding.

3.4 Conclusions

Three dimensional and real-time pore-level phenomena during the water invasion process in water-wet and oil-wet porous media were successfully visualized. To eliminate graphical errors, such as illusory oil/water films, that can be caused by X-ray broadening effects, the oil and water phases were carefully selected so that images produced using the X-ray CT scanner gave separate brightness distributions for each phase. In other words, the brightness of the fluids used bracketed the porous medium brightness. The boundary of each phase could then be determined with high precision, even in a single pore. The shape of the trapped oil and the interface between the water and oil were visualized clearly. Various phenomena that occur during water flooding in oil-wet and water-wet porous media were captured:

- The “overtaking-like” water invasion caused by different water invasion speeds in different channels, breaking the continuity of the oil phase, which is the most common oil trapping process in 3D porous media.
- An actual water film on the surface of the water-wet glass beads accumulated in the pore throat and snapped-off the continuity of the oil phase.

- The piston-like displacement process, which is the most common oil displacement process in porous media.
- The contact angle and pore throat radius were measured from direct observations, and used to calculate the capillary pressure during the snap-off and piston-like displacement processes in water-wet and oil-wet porous medium. From observation, piston-like displacement is more favorable, because, for a given pore throat radius, the threshold pressure is always higher for piston-like displacement than for snap-off.

4 PORE-SCALE INVESTIGATION OF THE EFFECT OF CONNATE WATER ON WATER FLOODING BEHAVIOR

4.1 Background

Water flooding is one of the most important processes in oil production. Water is injected into an oil reservoir to maintain the reservoir pressure, and the water sweeps some of the oil toward the production well. In the water flooding process, water displaces oil, a higher viscosity fluid, creating an unstable interface. Local heterogeneities in the porosity and permeability of the porous medium may enhance interface instability causing premature breakthrough of the displacing fluid at the exit of the porous medium and the displacing fluid flows preferentially through that established path. In actual oil reservoirs, *in situ* water, or connate water, is usually found (typically about 2%–5%) (Thibodeau et al., 1997). The existence of connate water also significantly affects water flooding and tends to reduce oil recovery by enhancing the instability of the displacement front. Usually less than 50% of the original oil in a reservoir can be recovered by water flooding. Capillary pressure holds trapped oil in pore spaces.

Numerous laboratory studies have been conducted to observe the water flooding phenomena with and without the presence of connate water. Some studies suggest that connate water adds additional perturbations to the displacement front, causing more irregular water fingering in oil–wet porous medium during water flooding (Paterson et al., 1984; Jamaloei et al., 2010). During water flooding, the connate water is displaced from the core and connate water bank accumulation is formed in front of the injected water, thus affecting invasion patterns (Graue et al., 2012). Connate water displaces in a piston-like displacement during spontaneous imbibition (Graue and Ferno, 2011). However, pore-scale description of connate water effects during water flooding in a three-dimensional (3D) porous medium is still unclear and limited.

Observation of water flooding as the pore-scale is usually conducted using micromodels (Chang et al., 2009; Jamaloei et al., 2010) or simulations (Blunt and King, 1992; Kang et al., 2004). Micromodels describe the water flooding process in two dimensions, and water flooding simulations require many parameters to be precisely determined. The recent development of microfocused X-ray computed tomography (CT) scanner technology allows nondestructive visualization of the phenomenon (Kumar et al.,

2010), and the technique's application allows observations critical to our understanding of fluid transport.

In previous two chapters, water flooding processes were visualized in water-wet porous medium and oil-wet porous medium. However, both chapters did not include discussion about the effect of connate water which always exists in actual oil reservoir. In this chapter, the effects of the existence of connate water on water flooding and oil trapping processes through a bed of packed glass beads by scanning the processes using a microfocused X-ray CT scanne were discussed. Water flooding experiments were conducted in a water-wet porous medium. The time-dependent processes, including the initial state, initiation of water invasion, invasion pattern, and trapping phenomena, were visualized clearly and step-by-step at the pore scale. The effect of connate water on residual oil saturation and local velocity of oil were also estimated.

4.2 Experiments

4.2.1 Experimental Scheme

Table14.1 Properties of fluids

Fluids	Composition	Density, g/cm^3	Viscosity, mPa·s
Water	Distilled water	0.998[a]	1.002[b]
Oil	Iodododecane 77 wt% + dodecane 23 wt%	1.031[a]	3.110[c]

[a]Measured at 20ºC

[b](Kestin et al. 1978)

[c]Measured with falling ball viscometer at 20 °C

Water flooding was visualized using a microfocused X-ray CT scanner (ScanXmate-G100S110; Comscantechno Co.). Recent developments in high-resolution X-ray CT scanners have enabled us to directly observe porous structures (Al-Raoush and Willson, 2005). The image resolution depends on the ratio of the distances between the X-ray source, detector, and object. The X-ray CT scanner produced images in gray scales, whose intensity is proportional to X-ray absorption. For the oil and water phases, iodododecane doped with 23 wt% dodecane and distilled water were used, respectively. The properties of these

phases are listed in Table 4.1. Glass beads fabricated from silica fibers with diameters of 350–500 μm (average 400 μm) were used in this experiment. The glass beads were washed with toluene, ethanol, and then water to remove the coating so that the glass beads became water-wet.

For the control experiment without connate water, a tube with an inner diameter of 10 mm and height of 60 mm was filled with oil, and the glass beads were gradually poured into it to avoid entrapping air. The section located in the middle of the tube, at a height of 10 mm, was the observed area; this area was scanned before beginning water flooding to determine initial conditions. Water was then injected upward at a capillary number Ca = 4.9 × 10^{-7} and the beads were scanned every 5 min for 1 h.

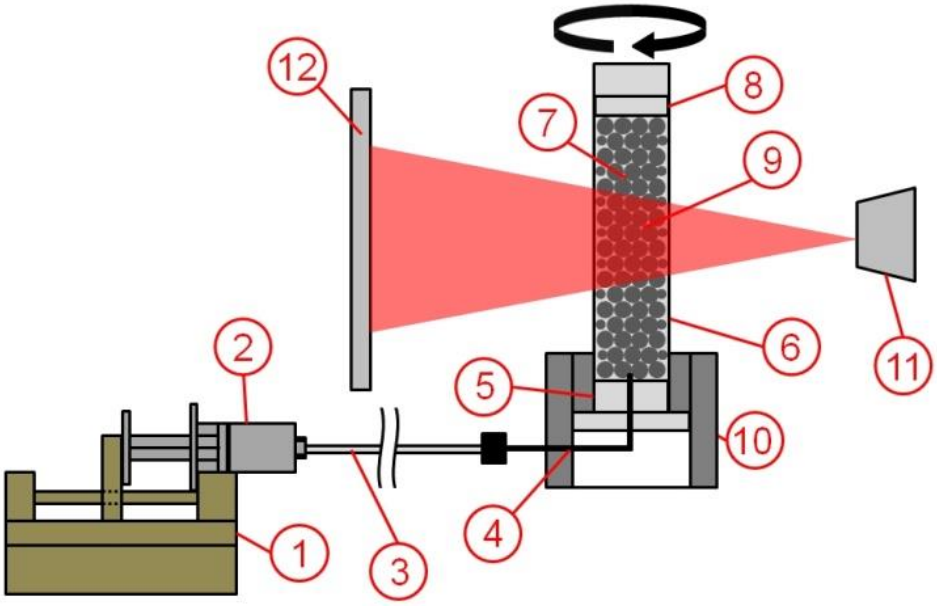

Fig. 4.1 Experimental setup. (1) Syringe pump, (2) syringe, (3) tubing, (4) needle, (5) bottom cap, (6) resin tube, (7) glass beads, (8) filter, (9) observed area, (10) holder, (11) X-ray source, (12) X-ray detector.

For the experiments in the presence of connate water, a tube with an inner diameter of 10 mm and height of 60 mm was filled with water, and the glass beads were poured slowly into it. Oil was then injected upward at Ca = 2.4 × 10^{-6} for 1 h, invading pores previously occupied by water. In this way, some water was entrapped, creating connate water for this

experiment. The observed area was the same as described above and scanning began once the oil reached the outlet but before water flooding began. Water flooding was then conducted by injecting water upward at Ca = 4.9×10^{-7} and the beads were scanned every 5 min for 1 h. The experimental setup is shown schematically in Fig. 1.1. The capillary number, Ca, is defined as the ratio of the viscous force to the capillary force at the pore scale (equation 4.1).

$$\mathrm{Ca} = \mu V / \gamma \qquad (4.1)$$

where V is the displacing phase velocity, μ is the water viscosity, and γ is the interfacial tension between the oil and water. The water invasion velocity was 1.1×10^{-5} m/s (11.1 cm/day). The interfacial tension between water phase and oil phase was 22.5 mN/m, as measured by the pendant drop method. At capillary numbers below 10^{-6}, the trapping mechanism is dominated by capillary forces, and the viscous force can be neglected (Morrow and Songkran, 1981).

4.2.2 Image Processing

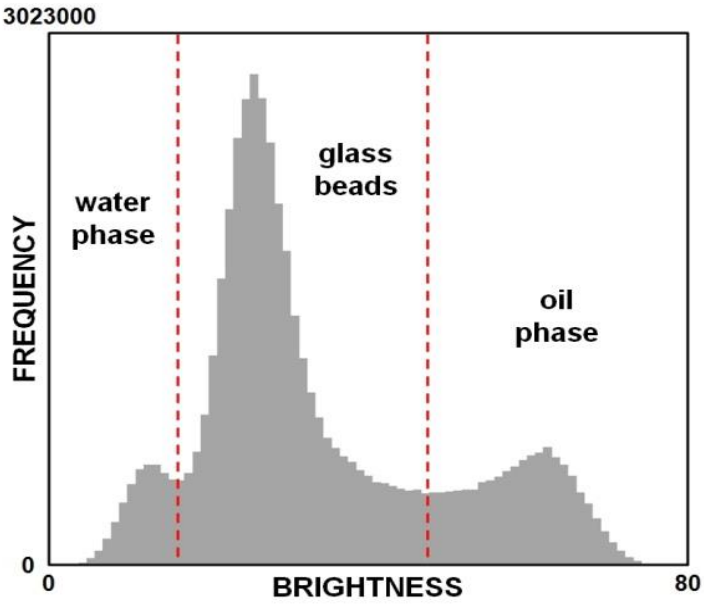

Fig. 4.2 Brightness intervals in the gray-scale images.

The maximum image resolution was 9.484 μm/pixel, and the scale, boundary, and optimum brightness were set using the image processing software Image J (Abramoff et al.,

2004). The glass beads, water, and oil were distinguished using appropriate brightness threshold values for each phase as shown in Fig. 4.2. Images from the image processing software were used to construct 3D images using the volume rendering software VG Studio Max 2.1. Images obtained at the initial conditions (in case of the experiment without connate water) or conditions after the water-filling process (in case of the experiment with connate water) were used to construct the glass bead structures for all data. Images from each time interval were used to digitally extract the water and oil phases independently. The glass bead structure was then combined with the water and oil phase images to create a complete structure at each time interval. Each phase can be digitally removed, if required.

Oil and water phases were carefully selected with two aims: to limit the buoyancy effect between the oil and water phases and to achieve the oil phase brightness such that the glass bead brightness lies between the oil and water brightnesses. A major consideration was the X-ray broadening effect. In images, the interface is broadened, creating a slope-like shape, decreasing the accuracy with which the boundary can be located, especially when phenomena in a single pore space are being observed. If the phase brightnesses are in the order water < oil < glass beads, broadening of the interface between the water and glass beads creates the illusion of an oil film on the surface of the glass beads. To eliminate this, each image set should have a reference image subtracted in order to digitally separate the oil and water phases. However, this is time consuming and leads to another error caused by improper subtraction, because of irregularities in the image sets.

4.3. Results and Discussions

4.3.1 Effect of Connate Water in Residual Oil Saturation

Figure 36 shows the decrease in oil saturation during water injection. The presence of connate water reduces oil recovery significantly. In case of the porous medium without connate water, average residual oil saturation was 24.67% (Fig. 4.3a). Oil saturation decreases gradually until steady state is reached, indicating stability of the displacement front. In case of the porous medium with connate water, reduction of oil saturation is dramatic (Fig. 4.3b). In the beginning, connate water saturation was 23.87%. After water flooding, average oil saturation reduced to 38.52%. When water first invades the porous medium containing connate water during water flooding, interstitial water hastens water-front progression, resulting in significant reduction of oil saturation within 5 min. When one water

finger reaches the outlet, the pressure gradient along this water finger significantly decreases. At that point, oil saturation is barely reduced until steady state is reached.

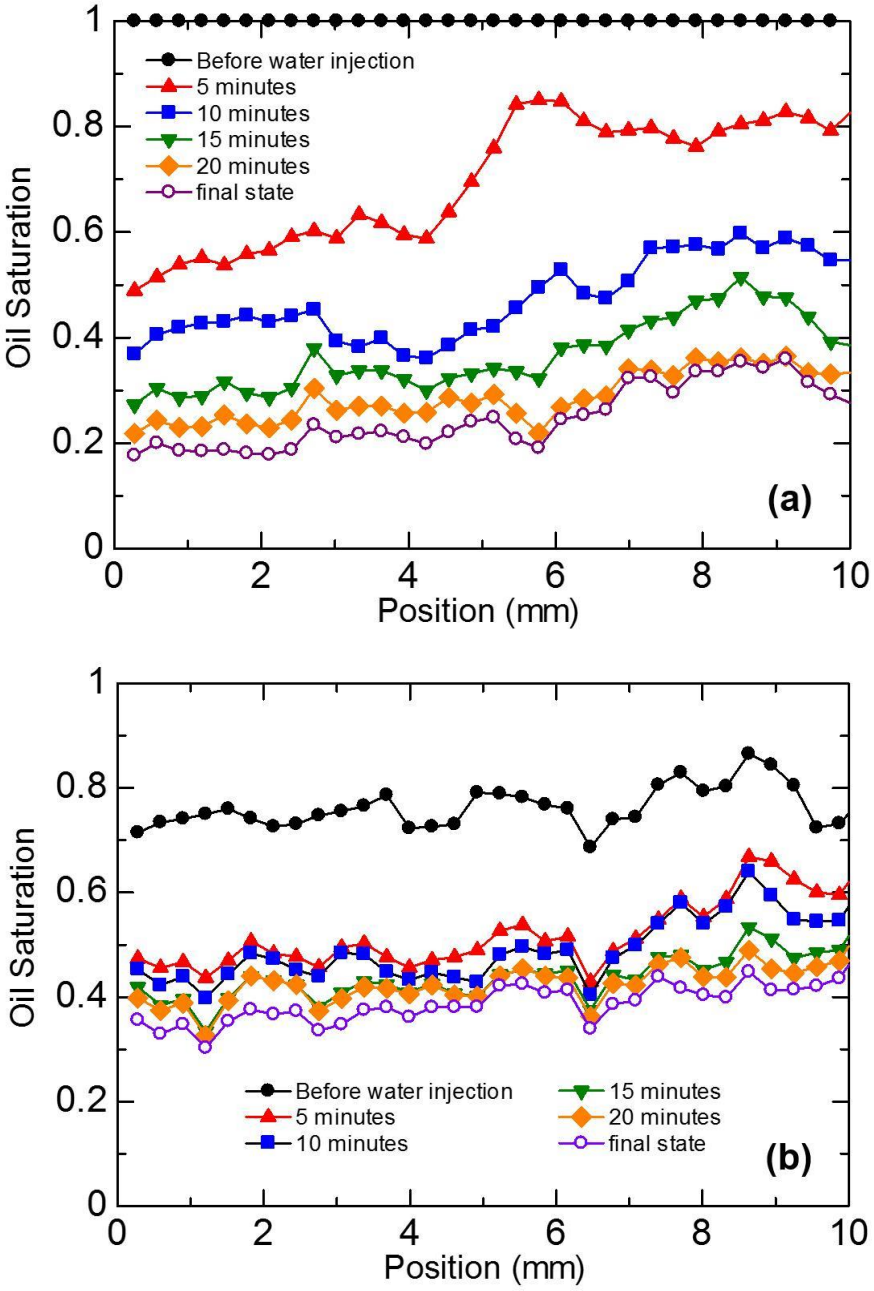

Fig. 4.3 Oil saturation change in porous medium during water flooding (a) without connate water and (b) with connate water.

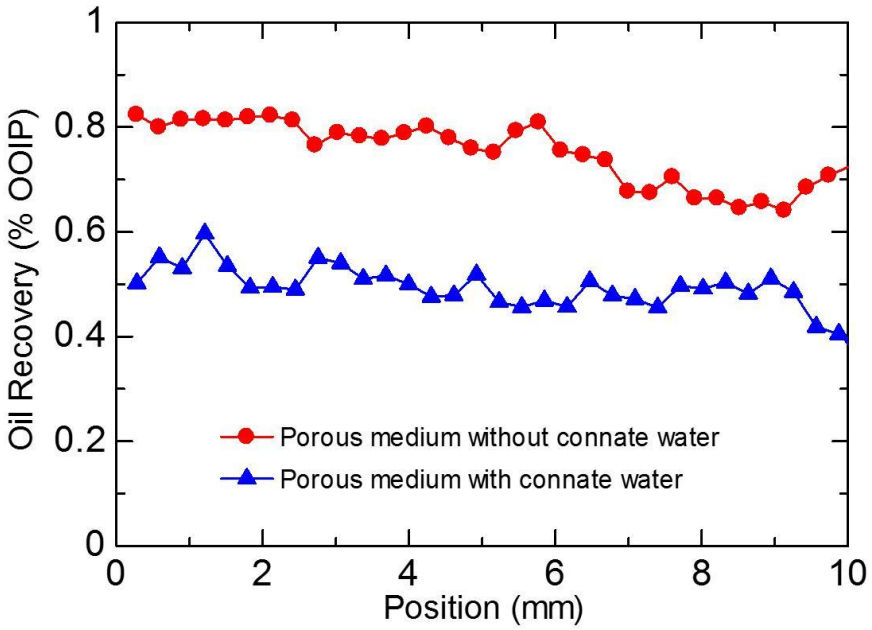

Fig. 4.4 Oil recoveries during water flooding in porous medium with and without connate water.

Figure 4.4 shows a comparison of oil recovery during water flooding for both porous media. Average oil recoveries in porous medium with and without connate water were 49.41% and 75.33% of the original oil, respectively. Clearly, the presence of connate water reduces oil recovery significantly.

4.3.2 Effect of Connate Water in Local Velocity of Oil

We apply a material balance approach (Goodfield et al., 2001), which can be expressed as

$$U_{oil}(z,t) = U(t)F_{oil}^{inj}(t) - \frac{\partial V_{oil}(z,t)}{\partial t} \qquad (4.2)$$

where $U_{oil}(z,t)$ is the local velocity of oil in the z position and at time t, $U(t)$ is the total fluid injection velocity in the inlet, and $F_{oil}^{inj}(t)$ is the fraction of oil in the inlet at time t. Oil volume

per unit cross-sectional area between the packed glass beads and position z, $V_{oil}(z,t)$, is defined by

$$V_{oil}(z,t)=\int_0^z \phi(\zeta)S_{oil}(\zeta,t)d\zeta \qquad (4.3)$$

where $\phi(\zeta)$ is the porosity of the porous media in specific positions and $S_{oil}(\zeta,t)$ is the oil saturation in specific positions at time t. Thus, the local velocity of oil at time t in specific positions can be summarized as follows:

$$U_{oil}(z,t)=\frac{V_{oil}(z,t)-V_{oil}(z,t+\Delta t)}{\Delta t} \qquad (4.4)$$

During injection of water into the porous medium without connate water, the local velocity of oil gradually reduces as the water invades the pore space (Fig. 4.5a); this is due to the steady interface movement. In case of the porous medium with connate water, the local velocity of oil reduces dramatically (Fig. 4.5b). When injected water comes into contact with connate water, the displacement front rapidly moves to the other end of pores containing connate water, which causes a jump-like movement of water. This phenomenon helps water to move faster and reach the outlet earlier than that in the porous medium without connate water. Consequently, in the same period of time, the amount of oil moved by water is less in the porous medium with connate water, leading to lower local oil velocity. Because of the jump-like movement in the porous medium with connate water, water breaks through within 0–5 min after the initiation of water flooding, and therefore, the local velocity of oil decreases significantly. This indicates that after water breakthrough, only a small amount of oil is produced. An oil velocity of 0 m/s indicates that oil has already been trapped.

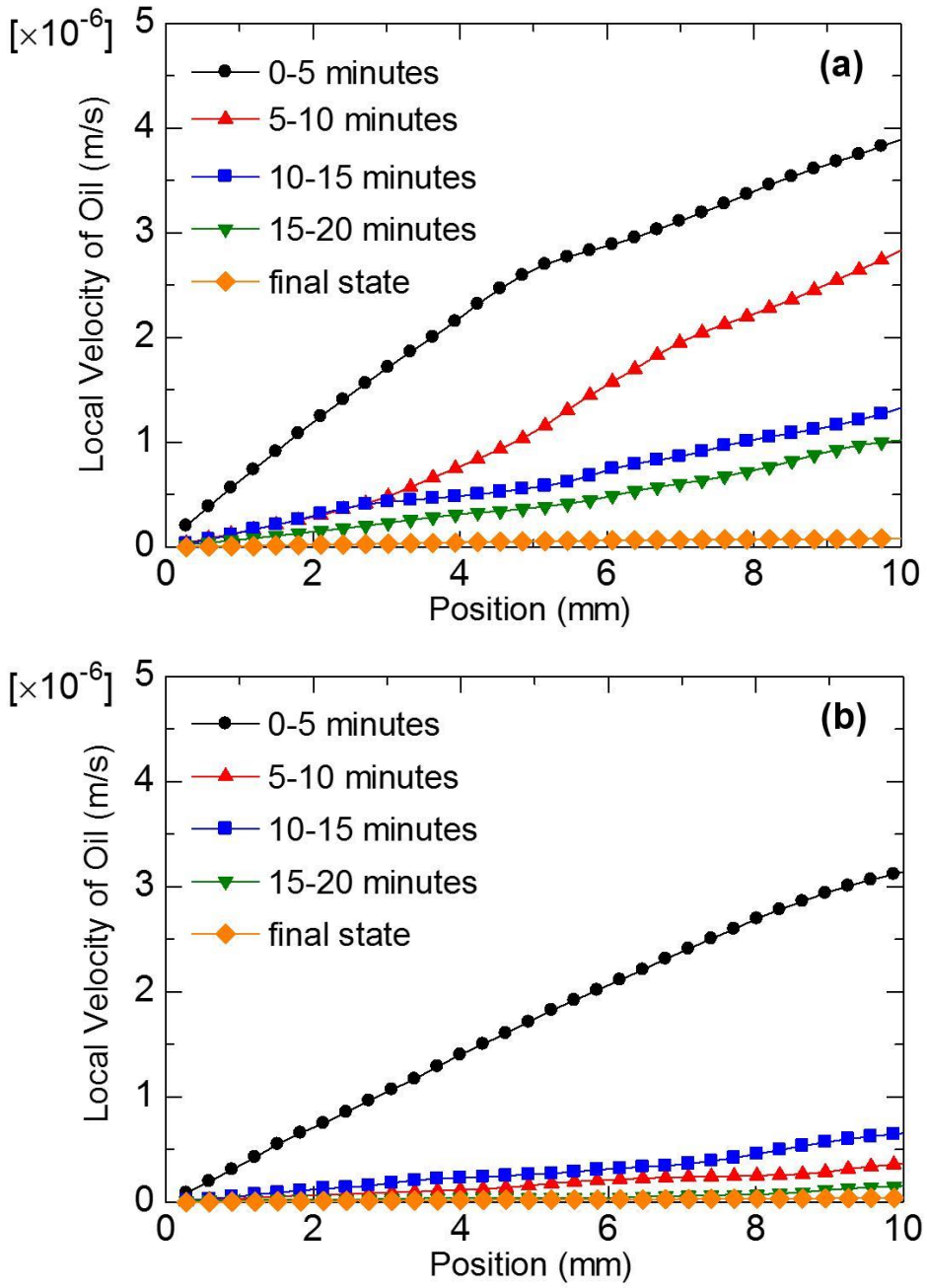

Fig. 4.5 Local velocity of oil in porous medium during water flooding (a) without connate water and (b) with connate water.

4.3.3 Effect of Connate Water in Water Invasion Pattern

Figure 39 shows water flooding in a porous medium without initial water saturation. The porous medium is digitally divided into one quadrant. The glass beads and oil phase are digitally removed to show how water invades the porous medium more clearly. The blue region denotes injected water. The water displacement front is dominated by a large single structure of water as shown in Fig. 4.6a. Water invasion into a water-wet porous medium containing oil can be considered as imbibition. In imbibition, water tends to flow through the smallest channel since it has the highest capillary entrance pressure, which helps it to invade the pores. Water is less viscous and has lower density than oil. Theoretically this condition should create perturbation on the displacement front, thereby creating smaller water fingers. All of those factors affect the stability of the displacement front and water's path; therefore, we can see in Fig. 4.6b that some oil was trapped. Fig. 4.6d shows that water successfully invades most of the porous medium, leaving 24.67% of the oil behind.

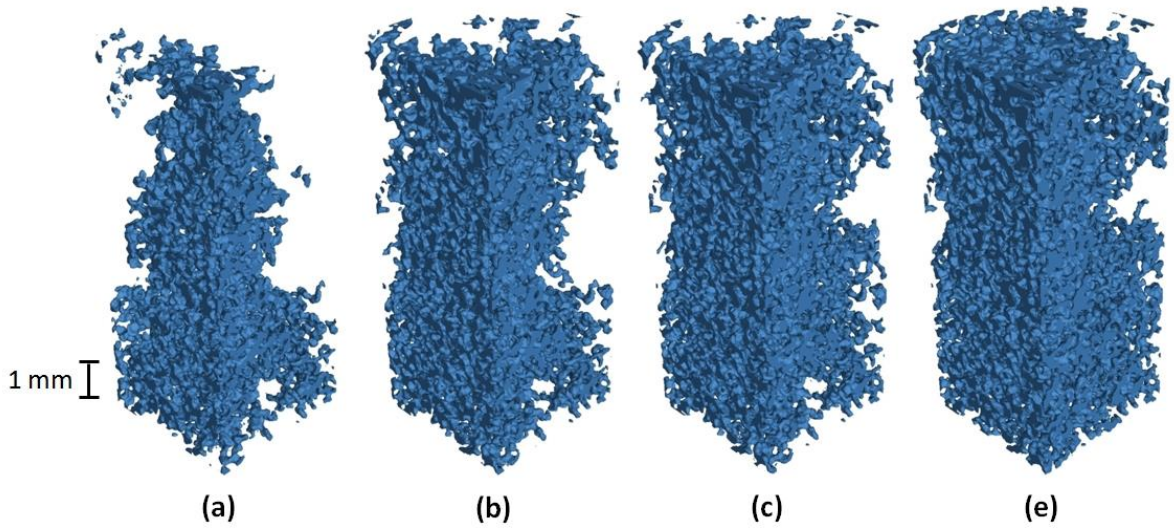

Fig. 4.6 Three-dimensional image of water flooding in porous medium without connate water. Following water injection for (a) 5 min, (b) 10 min, (c) 15 min, and (d) at steady state.

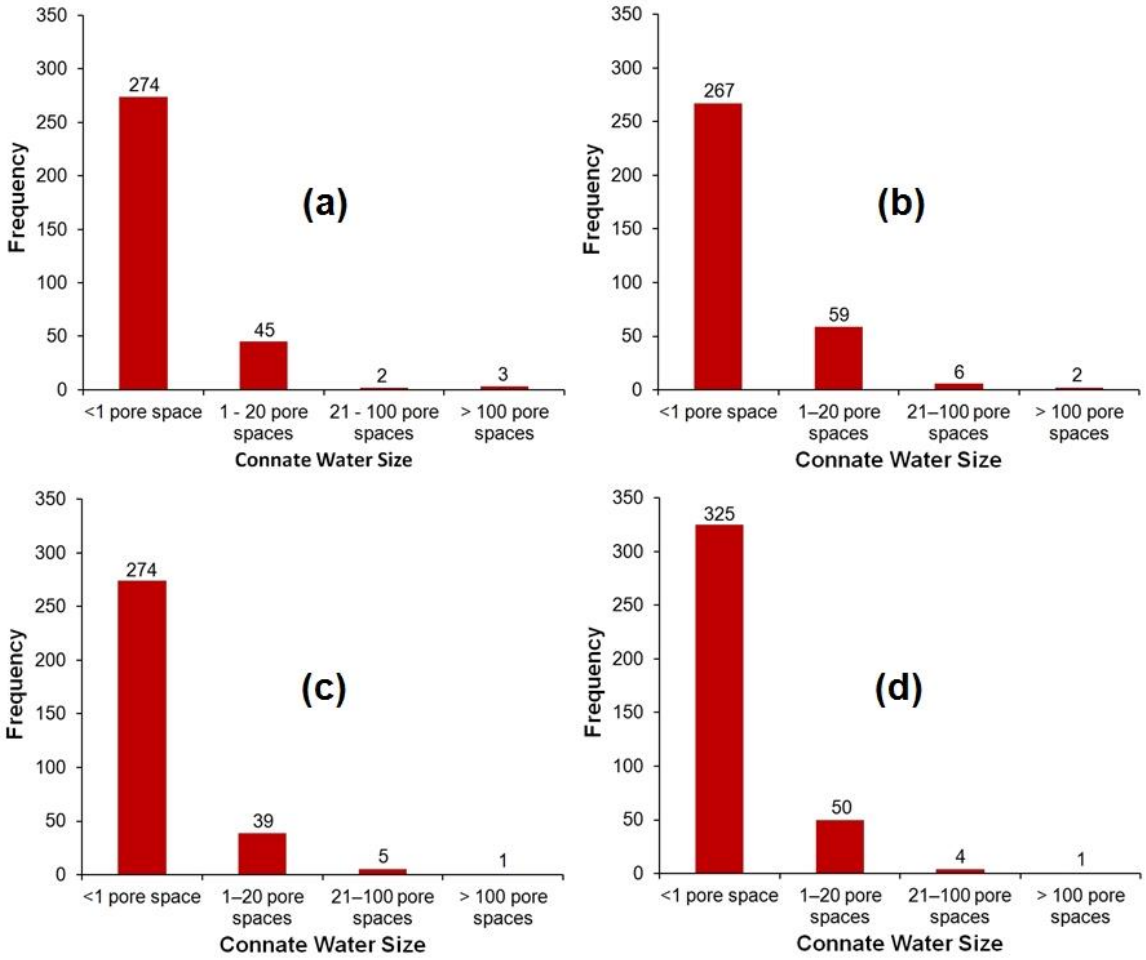

Fig. 4.7 Connate water sizes: (a) 0–2.5 mm, (b) 2.5–5 mm, (c) 5–7.5 mm, and (d) 7.5–10 mm.

For packed glass beads having diameters 400–600 μm (average 500 μm), the average pore body size was 57.8 μm (Al-Raoush and Willson, 2005). Pore body size for packed glass beads having diameters of 400 μm was estimated to be 46.24 μm. A volume of one pore space was estimated to be 0.4143 μm^3. By dividing the observed pores into four sections from bottom to top, connate water is then divided by size as shown in Fig. 4.7.

Figure 4.7 shows the distribution of connate water in pores of various sizes along the observed area. Seven large connate water channels with volumes of more than 100 pore spaces dominate the entire connate water. These large channels are surrounded by more than a thousand connate water channels in dispersed form, each of which has a volume of less than 1 pore space. Some connate water channels with volumes of several pore spaces

in a cluster of pores were also observed. From Fig. 4.7, we can see that the frequency distribution of connate water in various shapes along the pores is nearly even in each section.

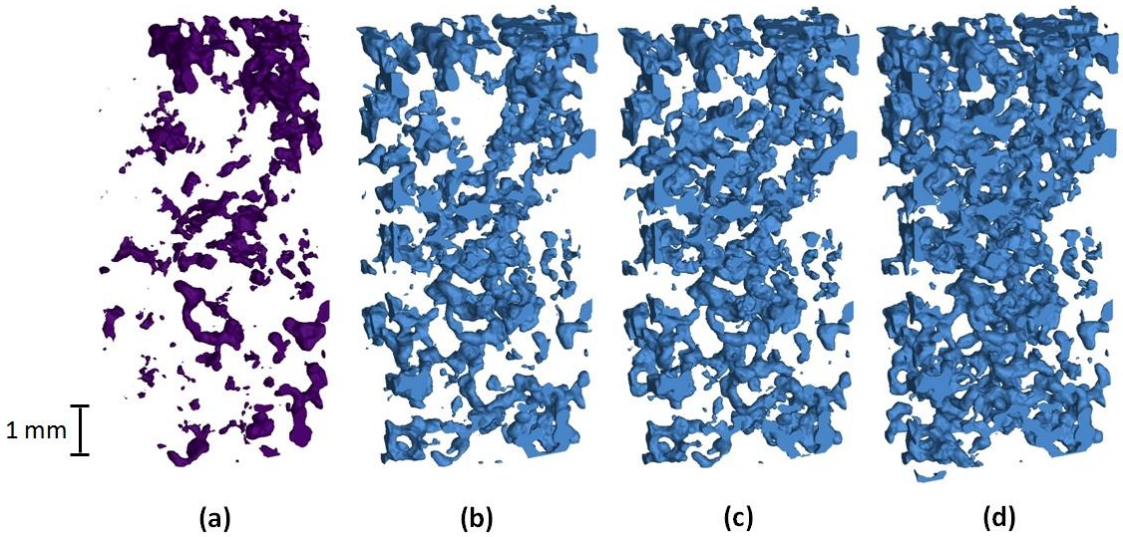

Fig. 4.8 Three-dimensional image of water flooding in porous medium with connate water: (a) initial condition, (b) injection of water for 5 min, (c) injection of water for 10 min, and (d) at steady state.

Figure 4.8 shows 3D images of water flooding in the porous medium with connate water. Three-dimensional porous media are very complicated structures. In order to show the effect of the presence of connate water on the development of water flow path during water flooding, the porous medium is digitally divided into 1 mm thick sections. Glass beads and the oil phase are also digitally removed. Purple and blue regions denote connate water and injected water during water flooding, respectively. Figure 4.8a shows the distribution of connate water along the observed area. Connate water exists in various forms and sizes.

In the beginning, the water invasion process has the same characteristics as that in the case of the porous medium without connate water; water tends to flow through the smallest channels in contact with the displacement front. Smaller channels provide higher capillary pressure, assisting spontaneous imbibition of water into pores occupied by oil. When injected water comes into contact with connate water, the displacement front rapidly

expands into that space. In this way, the front suddenly jumps ahead. Connate water exists in various shapes and sizes. When injected water comes into contact with connate water contained in pore clusters or with a volume of 100 pore spaces, the displacement front creates a jump-like movement. It expands dramatically and creates a severe water finger. The only pressure difference inside the tube is between the inlet and outlet, where the inlet is connected to a syringe pump and the outlet is at atmospheric pressure. When injected water contacts connate water, the shape of the displacement front abruptly changes. Before the contact, connate water constitutes a discontinued phase that is trapped by the capillary pressures of surrounding pores. However, when the both types of water come into contact, they have a continuous phase. Pores around connate water that previously created capillary pressure, holding connate water in place, now become the only way for the water phase to flow. Because a pressure gradient exists in the axial direction only, water tends to flow through the upper most part of that connate water and not in the radial direction. This is also the reason why injected water appears to flow faster toward the outlet in porous media containing connate water as opposed to porous media without connate water. During this process, the shape of connate water containing pore volumes may deflect the movement of injected water as shown in Fig. 4.8b. When dispersed connate water with volumes less than 1 pore space contacts injected water, it accumulates but does not tend to deflect the water flow path. Once water breaks through, the pressure difference significantly decreases and the water tends to flow through the established path toward the outlet.

Figure 4.8c shows a water flow pattern after water flooding is conducted for 10 min. The water phase that consists of connate water and injected water appears to grow thicker. In fact, it does not grow or expand radially because there is no pressure difference in that direction. The only reason the water channels thicken is that some other water fingers starting from the original location invade the channels next to the previous water finger so that it looks thicker. The water phase is slightly lighter and less viscous than the oil phase, because of which the displacement front tends to create many water fingers.

Figure 4.8d shows the condition of the porous medium at steady state. We can see that some parts of the media are not invaded by water and oil is trapped. Deflection of the water flow path upon contact with connate water can disrupt continuity and trap oil. Comparing the oil recoveries in case of the porous medium without and with connate water, it is obvious that connate water reduces oil recovery significantly, as discussed in previous sections.

4.3.4 Effect of Connate Water in Sweeping Efficiency and Distribution of Injected Fluid

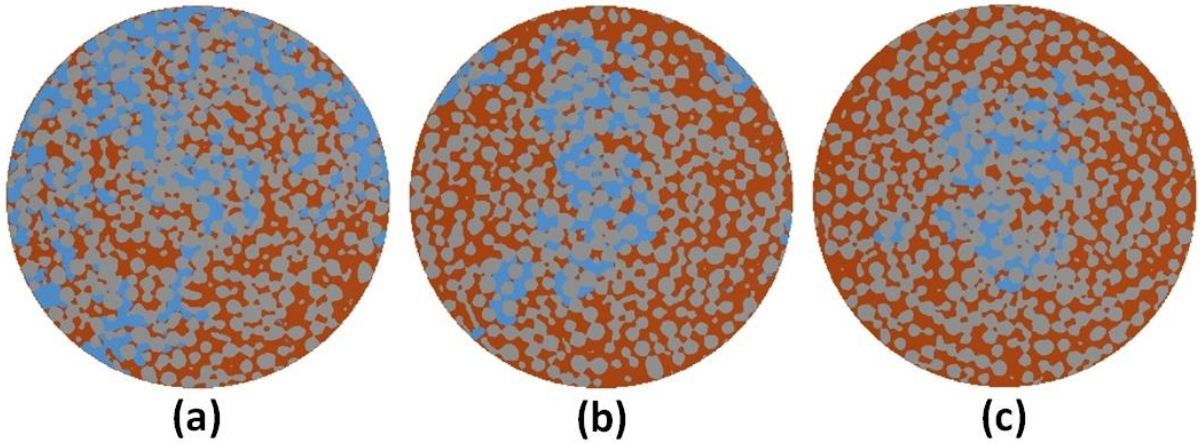

Fig. 4.9 Cross-sectional view of porous medium without connate water after water flooding for 5 min: (a) 0 mm, (b) 5 mm, and (c) 10 mm from the inlet.

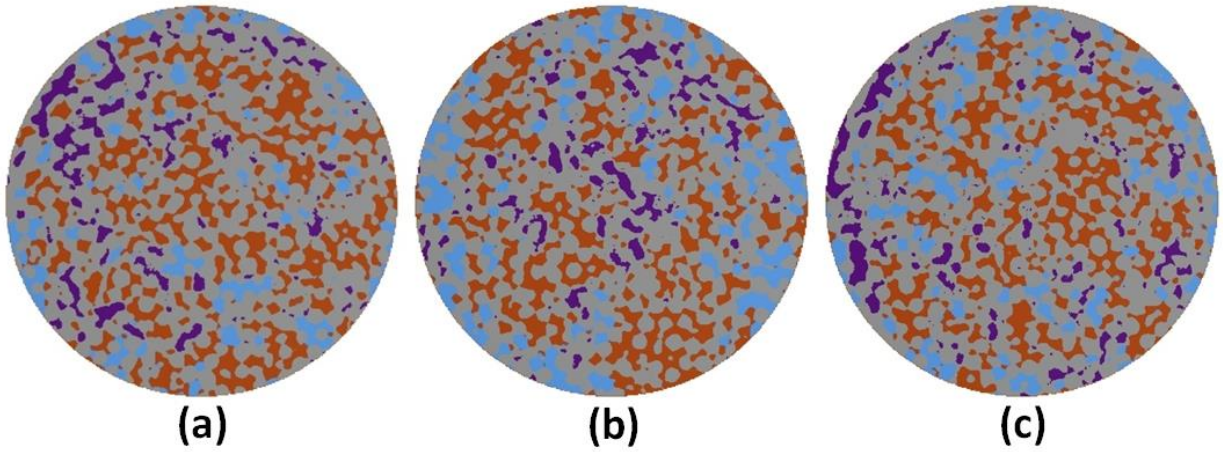

Fig. 4.10 Cross-sectional view of porous medium with connate water after water flooding for 5 min: (a) 0 mm, (b) 5 mm, and (c) 10 mm from the inlet.

Grey, orange, blue and purple denote glass beads, oil, injected water, and connate water, respectively. At 0 mm from the bottom of the observed area, injected water invades not only the area previously occupied by connate water but also neighboring channels, as shown in Fig. 4.10a. In Fig 4.9a, water saturation is 57.25%. In Fig. 4.10a, total area occupied by connate water and injected water is 47.78%, which constitutes 26.37% connate

water and 21.41% injected water. The water saturation in the porous medium without connate water is much larger than that in the porous medium with connate water. The existence of connate water reduces the growth of the area occupied by water, resulting in less sweeping area than in case of the porous medium without connate water, and this phenomenon is found even very close to the inlet.

At 5 mm from the bottom of the observed area, in case of the porous medium with connate water (Fig. 4.10b), saturation of injected water and connate water is 50.53%, constituting 20.63% connate water and 29.9% injected water. Comparing with Fig. 4.9b, water saturation is only 27.58%. At 5 mm from the bottom of the observed area, water saturation in the porous medium without connate water is actually less than in case of the porous medium with connate water.

At 10 mm from the bottom of the observed area, water saturation is 17.02% (Fig. 4.9c). Compared with Fig. 4.10c, the total water saturation is 38.03%, constituting 23.4% connate water and 14.63% injected water. This indicates that most water in the porous medium without connate water remains in the lower part of tube, sweeping larger area. While in case of the porous medium with connate water, connate water helps injected water to flow faster so that it reaches and occupies larger area in upper areas of the tube after 5 min of water injection. When connate water is present, water flows faster toward the outlet. So instead of sweeping more area at the 0 mm position from the observed area, most water reaches 5 mm and 10 mm above it.

4.4 Conclusions

This study successfully investigated three dimensionally the pore-scale behavior of water flooding in a porous medium with and without the presence of connate water. In the porous medium without connate water, water flooding was able to produce 75.33% of the original oil; approximately 1.5 times more oil that in the case of the porous medium with connate water. Because of the steady interface movement, the local velocity of oil reduced gradually with time as the water invaded the pore space. The water displacement front was dominated by very large water fingers, leading to better displacement stability. This stable displacement causes water to sweep more area but travel less far at a given time compared with the case of water flooding in a porous medium with connate water.

When water flooding experiment was conducted in the porous medium with connate water, water not only flowed through preexisting connate water but also occupied neighboring pores. However, only 49.4% of the original oil was produced. When injected water came into contact with connate water contained in pore clusters or with a volume of more than 100 pore spaces, the displacement front suddenly expanded and moved to the end of the connate water channel, leaving the other water fingers behind. Because the pressure gradient was present only in the axial direction toward outlet, this expanding displacement front tended to select pores closest to the outlet. The consequent jump-like movement helped water move faster and reach the outlet earlier than that in the porous medium without connate water. Water breakthrough occurred faster so the local velocity of oil was dramatically reduced. The shape of connate water may also deflect the movement of injected water, creating oil entrapment.

5 OBSERVATION OF WATER FLOW AROUND TRAPPED OIL BLOBS

5.1. Background

Fossil fuel continues to play important role in our energy supply. Generally, there are three stages to recover oil from reservoir rock; primary recovery, secondary recovery, and tertiary recovery. Primary recovery relies on natural mechanism such as gravity drainage and expansion of gas inside reservoir rock. Secondary recovery is a term usually used for describing injection of additional fluid to maintain the reservoir pressure. In many cases, water is used as injected fluid so that we called as water flooding. Injected water will sweep some additional oil towards production well. Unfortunately, during its process, some oil blobs are discontinued due to uneven invasion of water and they are trapped. During the primary production of oil and the application of water flooding, at least 50% of oil remains in the reservoir (Blunt et al. 1993). To recover such oil, oil companies usually conduct tertiary recovery; injection of additional sweeping agent (surfactant, bacteria, steam, etc) whose job is to increase the mobility of trapped oil by reducing the interfacial tension holding oil blob in pore space. Tertiary recovery will only extract some additional oil; usually extracts 60% – 70% of total oil. If we cannot produce most trapped oil, it means that the sweeping agent is unable to make contact with trapped oil blobs located in pore space. The existence of oil blobs may cause such a disturbance in the flow field of injected fluid, but there is no strong evidence of it.

Water flooding and surfactant injection have been subject of extensive studies by the petroleum production industry in the past and are currently of even greater interest as because of critical need to improve recovery efficiency from petroleum reservoirs. Literature related to this field is large, and yet incomplete, since the direct observation in actual case is too complicated. Scientists usually conduct observation in 2D porous medium in laboratory-scale (Chang et al. 2009; Jamaloei et al. 2010; Lenormand 1990; Jamaloei and Kharrat 2012) or simulation (Blunt and King 1992; Kang et al. 2004; Lenormand et al. 1998). However, we need more realistic description. There are many differences between 2D porous medium and 3D porous medium concerning porous structure that may affect the detail of multiphase flow mechanism. Assumption made in making simulation sometimes lead to different phenomena with actual case. Recent advances in high-resolution 3D

tomography have allowed researchers to non-destructively observe porous media systems (Lindquist and Venkatarangan 1999; Al-Raoush and Wilson 2005; Wildenscheld 2002).

In previous three chapters, water flooding processes have been observed in water-wet and oil-wet porous medium with variation in the existance of connate water. However, discussion about how water behaves when it flows through porous medium after oil entrapment is still unclear. Why oil production decreases after oil is trapped, why injection of more water cannot extract trapped oil blob, and why injection of surfactant in tertiary recovery process cannot produces 100% trapped oil; are still unclear. Observation of water flow field around trapped oil blob in pore-scale is highly necessary.

In this chapter, water flow field around the trapped oil blobs was observed from the microscopic point of view. The velocity averaged over the blob volume should be zero and water around trapped oil blob should be stagnant. Injection of additional water after water flooding may not be able to make a direct contact with trapped oil blob because of this stagnant water phase. In this research, we utilized packed glass beads as artificial porous medium to observe experimentally the stagnant region around trapped oil blobs. We scanned it by micro focused X-ray CT scanner and get high resolution image so that the pore-scale event can be seen clearly.

5.2 Experiments

5.2.1 Experimental Scheme

Comscantechno Co., ScanXmate-G100S110 was utilized as X-ray CT scanner. The image produced by the X-ray CT scanner was a gray-scale and its resolution depends on the distances among the X-ray source, detector, and object. To clearly observe the multiphase phenomena, phases with different X-ray absorption properties were used, so that their brightness in the gray-scale image was distinct and could be differentiated by determining its minimum and maximum brightness. Images resolution was 30.428 μm/pixel. The scale, boundary, and optimum brightness were set by using Image J (Abramoff et al. 2004).

Iododecane doped by dodecane 23% by weight was used as oil with combined density 1055 kg/m^3 and viscosity 3.110 mPa·s. We injected primary water (PW) that is water doped by NaI 7.5% by weight with combined density 1055 kg/m^3 and viscosity 1.002 mPa·s. To trace water flow around trapped oil blob after water flooding, we used pure water with

density 998 kg/m^3 and and viscosity 1.002 mPa·s as secondary water (SW). For porous media, we utilized oil-wet glass beads fabricated using silica fibers, 350 – 500 µm (average 400 µm) in diameter, packed in an acrylic resin tube with 10 mm in diameter and 40 mm in height. To avoid entrance and end effect, scanned area was located approximately in the middle of the tube with 10 mm in height.

All injections were conducted by using a high-accuracy, low-rate pump (KDS-210, kdScientifc) so that we can get constant injection flow rate. In theory, water invasion process in porous medium is determined by the competition between viscous and capillary forces that is represented by the capillary number. In this experiment, the capillary number Ca was defined as the ratio of the viscous force to the capillary force in the pore scale:

$$\mathrm{Ca} = \mu V / \gamma \qquad (5.1)$$

where V is the displacing phase velocity 1.06 × 10^{-5} m/s, µ is the water viscosity 1.002 mPa·s, and γ is interfacial tension between water phase and oil phase 22.5 mN/m; therefore, *Ca* was 4.7 × 10^{-7}. If *Ca* is lower than 10^{-6}, the trapping mechanism will be dominated by the capillary force, and theoretically, the viscous force can be neglected (Morrow and Songkran 1981)).

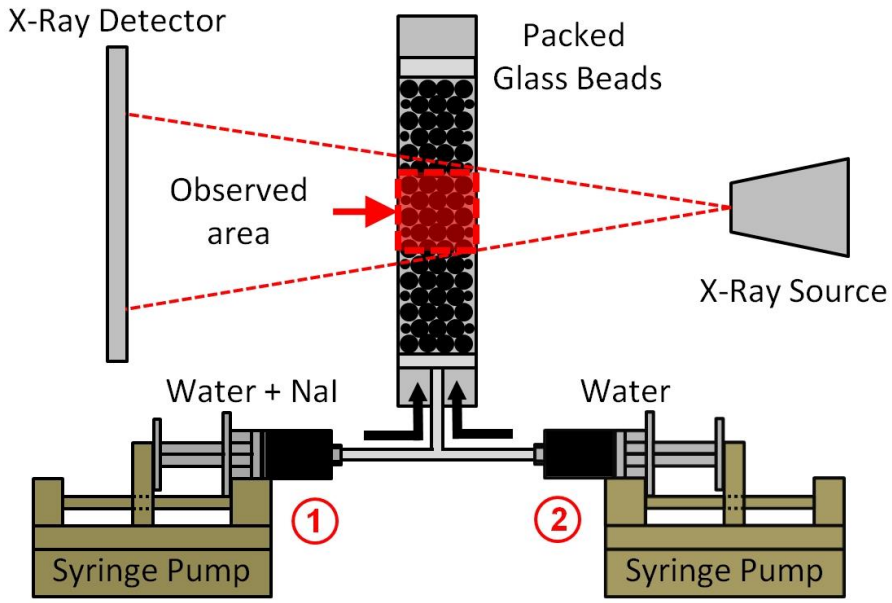

Fig. 5.1 Experimental setup.

We filled tube with oil and added the glass beads slowly in order to avoid air entrapment. The porosity of the packing was 38.2%. We scanned initial condition of packed

glass beads, then injected PW upward with $Ca = 4.7 \times 10^{-7}$ and scanned every minute until 3 pore volumes. Pore volume is defined as the volume fluid that will completely fill all of the void space in a given volume of porous matrix. In our case, for observed area of 10 mm in diameter and 40 mm in height, 1 pore volume was 1.194 ml. With injection flow rate 3 ml/h, 3 pore volumes will be reached after 72 minutes of injection. Scanning process took approximately one minute. Oil blobs appeared stationary in the X-ray CT monitor because interfacial tension held them in pore space. Then we injected SW with the same *Ca* and scanned every one minute and stop after injection for 3 pore volumes. Data taken during first and second injection were compared. Which such *Ca*, we can catch the process of SW invasion step by step clearly and reducing observation time so that blur on image due to dispersion of SW to PW can be reduced.

We determined water doped by NaI as PW because we want to reduce the gravitational effect during oil trapping process. By injecting PW having nearly same density with oil, the phenomena is assumed not affected by gravitational force. Pure water as SW was chosen based because it has different X-ray mass attenuation coefficient with PW so that it shows different level of brightness.

5.2.2 Image Processing

To observe the water flow arround trapped oil, we compared the brightness change of some selected pores representing the concentration of NaI in it. We injected PW until the system reached steady state and PW occupied the rest of area with almost constant brightness. From histogram, average brightness of pores occupied by PW can be obtained. The reason of high brightness value is NaI contained in PW. During SW injection, some pores will be invaded. When SW invades pore space, concentration of NaI in it will be reduced because SW itself is pure water without NaI. From the image produced from X-ray CT scanner, pores invaded by SW will show darker color. How SW flows arround trapped oil can be analyzed by observing how brightness was reduced in each scanning process. Reduction of NaI will correlate with the amount of SW invaded that observed pore.

Based on histogram of pictures produced by X-ray CT scanner, the brightness range is between 0 (black) and 255 (white). First, brightness of selected pore before injection of PW was measured and denoted as X_0 representing condition with 0% NaI (brightness value is almost 0). Then brightness of pore occupied by PW after injection for 3 pores

volumes was measured and denoted as X_p representing brightness of pore having 7.5% NaI in it. Then brightness when SW invades porous medium for n minutes was measured and denoted as X_s. From those data, calculate NaI concentration in observed pore of *n* minute injection of SW can be calculated and denoted as C_n

$$C_n = \frac{X_s}{X_p - X_0} \times 7.5\% \qquad (5.2)$$

5.3. Results and Discussions

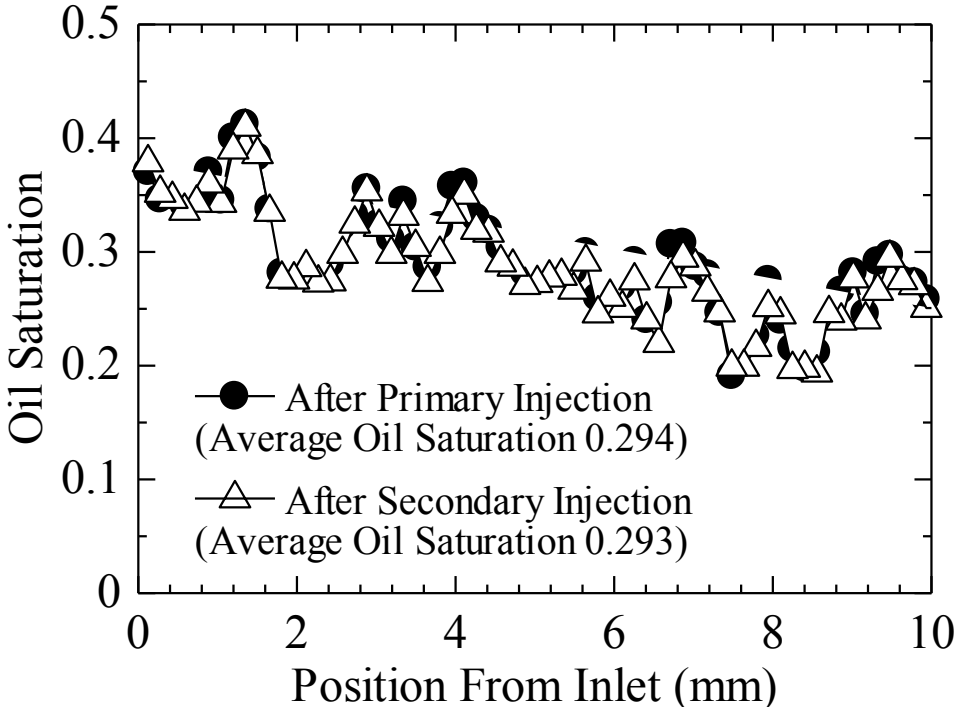

Fig. 5.2 Oil saturation after PW and SW injection.

Figure 5.2 shows oil saturation after PW and SW injection. Oil saturation was calculated from the total volume of trapped oil in observed area compared with the total volume of pore space there. From tube with 40 mm in height used in this experiment, our observed area was 10 mm located in the middle of it. There is no significant difference of oil saturation after PW and SW injection meaning that the SW flow field will not be interrupted by oil movement. Because each fluid was carefully selected, each phase can be seen clearly

in X-ray CT scanner. At the beginning, we scanned packed glass beads containing only oil as shown in Fig. 5.3a. Black and white denotes oil and glass beads respectively. Then PW was injected (denoted by light grey) in upward direction for 3 pore volumes resulting oil entrapment and then scanned it as shown in Fig. 5.3b. This PW acted as water flooding process in actual oil reservoir. Oil saturation in packed glass beads was 29.4%.

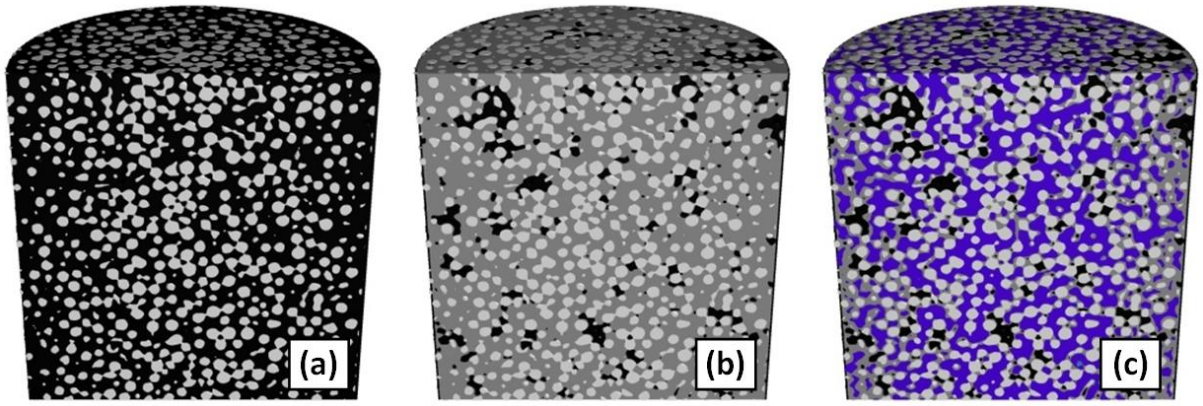

Fig. 5.3 (a) initial state (b) PW injection (steady state) (c) SW injection (steady state).

Water invaded into pore space at different invasion rate due to capillary pressure depending on pore diameter. Because displacing fluid is less viscous than displaced fluid, viscous fingering will create inhomogeneous interface. Because of over-taking like maneuver of water invasion, some oil blobs will be discontinued and trapped by capillarity. Some small oil blob and cluster-size oil blob are observed in Fig. 5.3b. We can neglect the effect of gravity because PW and oil have nearly same density.

After that SW (denoted by dark grey region) was injected acting as tracer to find out the distribution of water around trapped oil blob as shown in Fig. 5.3c. Injection of SW was conducted after PW was injected for 3 PV, so we assumed that the flow field around trapped oil blobs has been fully developed. The velocity averaged over the blob volume should be zero. From Fig. 5.3c, SW seems to invade most pores homogenously. Compared with 2D porous medium, condition in 3D porous medium is quite different. The network in 2D porous medium can be considered as lattice. Coordination number in this porous medium can be varied from only one to unlimited. In 3D porous medium, the coordination number can be multiplied because it has not only single lattice, but it consist of stack of lattices. Because of that during invasion of water whether it is PW or SW, water has more

paths to be selected in 3D porous medium than that in 2D porous medium. Because there are more alternative paths, during SW injection, SW was able to minimize severe water fingering and able to spread well throughout porous medium. By magnifying some observed pores, we were able to observe the detail of the condition around trapped oil blob as shown in Fig. 5.4 and Fig. 5.5.

5.3.1. Visualization of Water Flow around Trapped Oil Blob

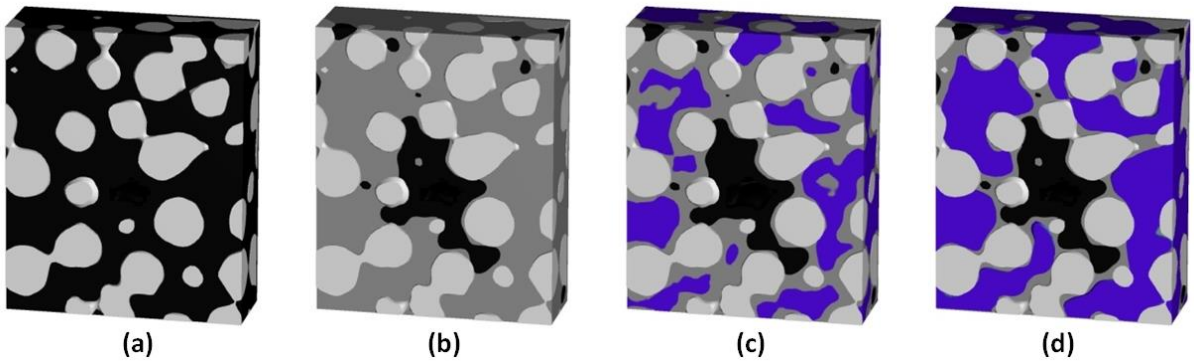

Fig. 5.4 Observed oil blob (a) before PW injection (b) 3 minutes injection of PW (c) 5 minutes injection of SW (d) steady state.

Figure 5.4 shows magnification of the oil blob. Initial condition with the oil saturation of 100% was shown in Fig. 5.4a with black and white region denote oil and glass beads respectively. After injection of PW for 3 PV, some oil blobs are trapped and one of them is shown in Fig. 5.4b. Light grey region denotes PW. With this level of magnification, the shape of oil blob can be observed very clearly. In this experiment, we injected SW with controlled flow rate and scanned it every one minute. Figure 5.4c shows the condition after injection of SW for 5 minutes. Dark grey region denotes the area invaded by SW. From this figure, we can see that SW was able to invade pores located just next to trapped oil. Closer inspection suggest that, even though SW invaded adjacent pore, there is a stagnant water film from PW that prevent direct contact between trapped oil and SW. Injection of SW for 3 PV as shown in Fig. 5.4d emphasize that finding. We can see clearly that, there is very tiny part of PW surrounding trapped oil which is unable to be displaced and invaded by SW. Stagnant water film existing between trapped oil and SW was less than one pore size.

In actual oil reservoir, in order to produce trapped oil with injection of surfactant, surfactant has to make a contact with trapped oil so that the interfacial tension that hold oil blob in pore space can be reduced and it will be easier for such oil to be extracted. From Fig. 5.4, we can see that there is stagnant water film from PW separating trapped oil blob and SW. In this case SW was injected after oil is already trapped. In actual oil reservoir, surfactant is also injected after oil is already trapped after water flooding. If several pores or even tiny stagnant water film separate surfactant and trapped oil, there will be only two ways for surfactant to reach that trapped oil; by molecular diffusion and convection. In such a condition, injection of surfactant will not be effective to produce trapped oil.

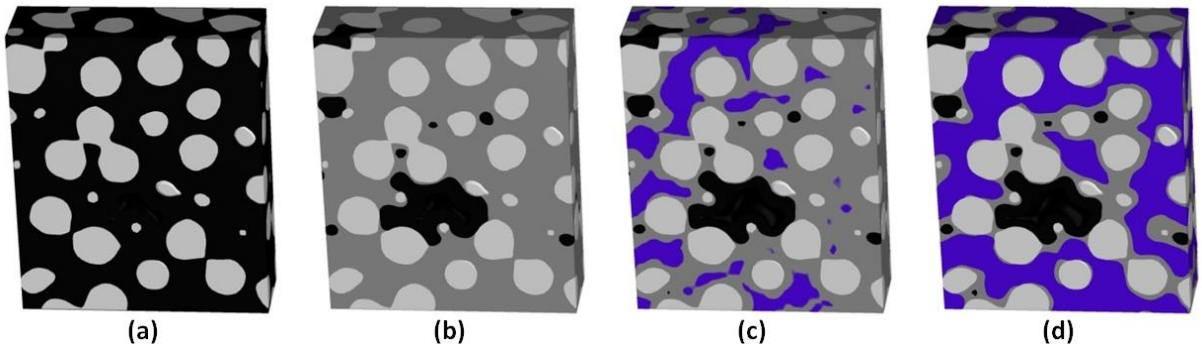

Fig. 5.5 Observed oil blob (another position) (a) before PW injection (b) 3 minutes injection of PW (c) 5 minutes injection of SW (d) steady state.

To make sure about this finding, we observed another trapped oil blob as shown in Fig. 5.5. Initial condition was shown in Fig. 5.5a with black and white region denote oil and glass beads. Injection of PW for 3 PV caused oil to be trapped as shown in Fig. 5.5b. Light grey region and dark grey region denote PW and SW respectively. When we injected SW for 6 minutes, some SW was able to invade adjacent pore as shown in Fig. 48c. The condition is exactly same with Fig. 5.4 that even though SW was able to invaded pores located next to trapped oil blob, but there was a stagnant PW preventing their direct contact. By comparing Fig. 5.4 and Fig. 5.5, we believe that this situation is not coincidence and also has a possibility to occur in actual oil reservoir. Different porous structure may create some variations, but at least this observation gave better perspective about inefficient process of surfactant injection with several assumptions and analogies.

In this case, PW and SW are miscible fluids. When two immiscible fluids are in contact, they will slowly diffuse into one another. The diffusion flux depends on diffusion coefficient, concentration, and distance. The diffusion process can disturb the visualization of the interface between trapped oil and SW. However, our experiment has very short interval of time. Even we observed the condition in every minute so that the effect of diffusion can be reduced. Beside diffusion, there is also dispersion that occurs when two immiscible fluid flow together in porous medium. This mixing process occurs in longitudinal and transverse directions. However, with such a small *Ca* and radius of the channel, dispersion effect can also be reduced.

5.3.2. Observation of Water Flow in Selected Pores by Brightness Analysis

We also conducted brightness analysis of some selected pores located around trapped oil blob to get better understanding about the flow behavior of SW more quantitatively. We divide the position of pores surrounding trapped oil into upstream, downstream, right side, and left side pores as shown in Fig. 5.6. Pores in the upstream side were A, B, and C. Pore in the right side were D, E, and F. Pore in the downstream were G, H, I, and J. Pores in the left side were K, L, M, and N. We separated the observation into several groups to compare how trapped oil blob affect flow distribution of SW.

In this experiment, SW was injected and it will displace PW on pore space. During its displacement, the concentration of NaI (7.5%) from PW will be reduced causing a reduction of brightness value. By comparing the way NaI concentration decrease, we can predict the flow behavior of SW around trapped oil blob as shown in Fig. 5.7 and Fig 5.8.

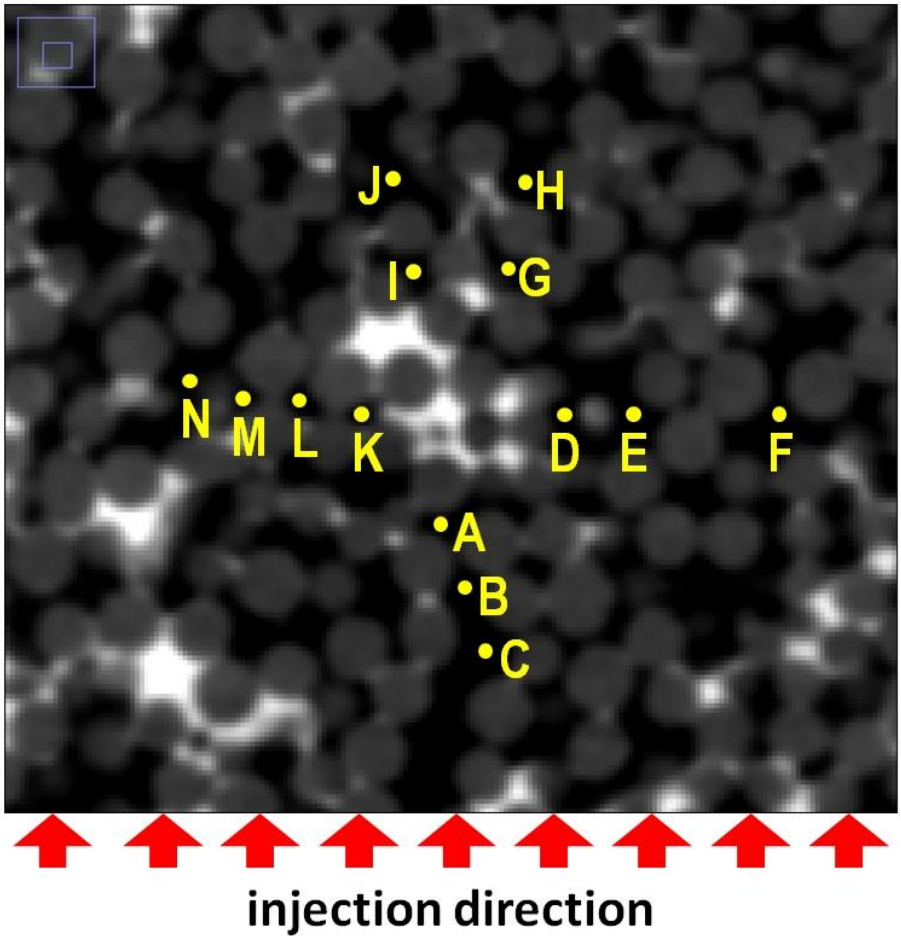

Fig. 5.6 Observed pores around trapped oil blob.

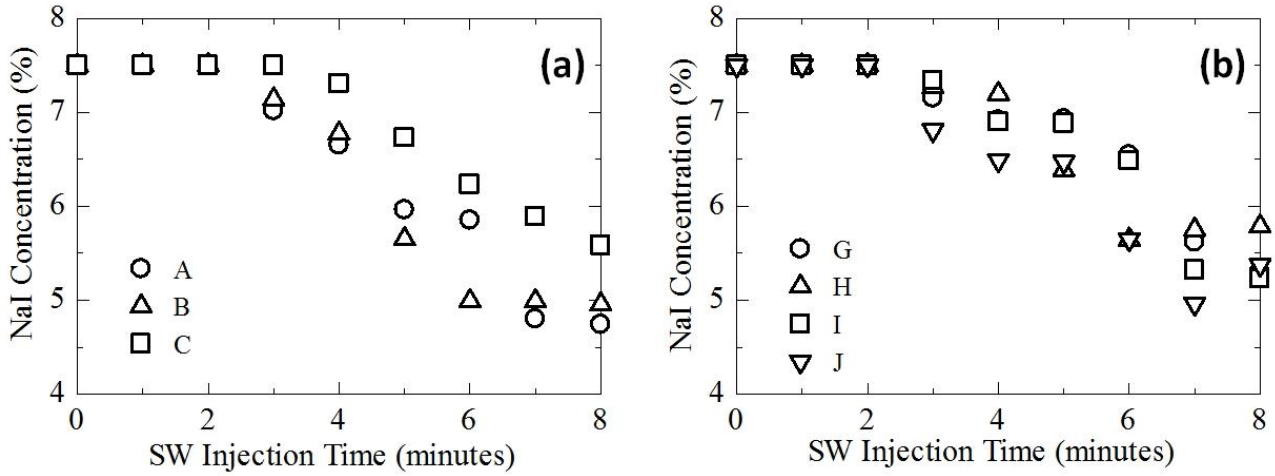

Fig. 5.7 NaI concentration in the neighboring pores (a) upstream (b) downstream.

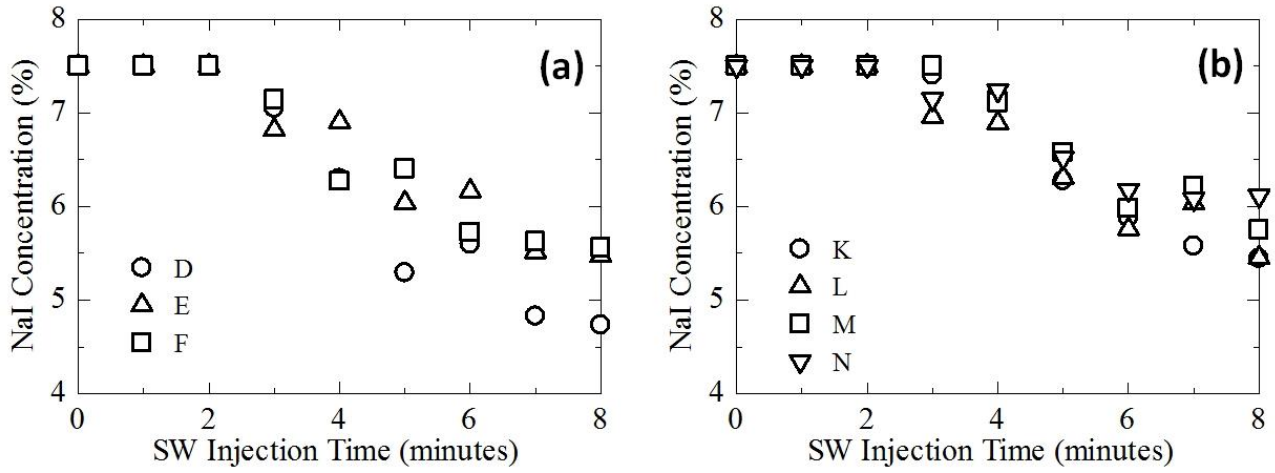

Fig. 5.8 NaI concentration in the neighboring pores (a) right side (b) left side.

Figure 5.7 and 5.8 shows NaI change during invasion of SW in observed pores. Reduction of NaI concentration in upstream pore was shown in Fig. 5.7a. From that figure, we can see that NaI concentration was reduced almost simultaneously with no distinctive difference in reduction pattern. In pore A which is located just next to the trapped oil blob, the NaI reduced with no delay or some strange pattern. At the beginning, we expected that the existence of trapped oil blob will give significant effect in SW flow field that in upstream pore, several pores from trapped oil blob, SW flow could be deflected, similar in the case of 2D network model observation (Suekane and Tezuka 2013)). In packed glass beads observation, the area affected by oil blob existence is not significant, less than 1 pore size.

Reduction of NaI concentration in downstream pore was shown in Fig. 5.7b. Again, similar with upstream pores case, SW managed to invade pore located just next to trapped oil. It means that, after passing the trapped oil acting as obstruction, SW regained its flow path immediately with no separation. The process of invasion and displacement of oil by PW in oil-wet glass beads can be considered as drainage process. In drainage, PW will prefer to flow through larger pore because it has less capillary pressure acting as resistance of PW flow. Invasion of SW into pore previously occupied by PW can be considered as single phase transport. Permeability in larger pores is bigger, so that SW will flow faster in larger pores previously occupied by PW. Also there are effects caused by diffusion and dispersion. All of those factors are combined and create a small variation as observed in Fig. 5.7. We can see that the NaI reduction timing and magnitude of concentration reduction are not same for all pores.

Figure 5.8 shows reduction of NaI concentration in pores located right and left side. In Fig. 5.8a, the diameter of channels in pores D, E, and F were 195.42 µm, 323.66 µm, and 390.13 µm respectively. Comparing the NaI concentration from 3 minutes to 8 minutes, reduction of NaI in pore D is bigger than others because of non uniformity of channel surrounding blob. When SW in one channel are blocked by oil blob, velocity of stream line will be deflected resulting in various velocity directions and it has to find other way to flow, SW will choose channel having closer distance with the deflection point. In Fig. 5.8b, we compared the NaI concentration in pores having distance 1 to 4 pores from trapped oil. The diameter of channels in pores K, L, M, and N were 152.67 µm, 189.31 µm, 137.41 µm, and 274.81 µm respectively. Even with a such a variation in channel diameter and distance to the trapped oil blob, again, SW managed to invade all of those pores almost homogenously. From Fig. 5.8, we can say that SW was able to invade pores located just next to trapped oil.

5.4 Conclusions

From direct observation of condition around trapped oil blob, we have several new findings.

a) We were able to visualize three dimensional water flow phenomena around trapped oil blob by utilizing water doped by NaI as replication of water flooding and pure water as tracer showing its flow pattern around trapped oil blob.
b) In 3D porous medium, after water flooding process, injection of additional miscible fluid was able to invade most pores almost homogenously. No significant effect of the existence of trapped oil to deflect the flow field.
c) Additional miscible fluid (SW) injected after water flooding process was able to invade pores located just next to trapped oil. However, in closer inspection, it seems that there is a small amount of stagnant water film comes from water flooding process (PW), that prevent the contact between SW and trapped oil. The size of stagnant PW in unconsolidated packed glass beads case was less than 1 pore size. We believe that the situation in actual oil reservoir may be similar that stagnant water film exists after water flooding. This stagnant water from water flooding process will act as a barrier preventing the contact between surfactant and trapped oil blob in tertiary recover process, thus reducing significantly the effectiveness of surfactant injection. Surfactant will be able to

make direct contact with trapped oil blob only by means of molecular diffusion and convection.

4 CONCLUSIONS

In this research, water flooding and oil trapping processes were described comprehensively in packed glass beads by utilizing micro focused X-ray CT scanner. We developed visualization scheme which made us possible to clearly observe water flooding process and oil trapping mechanism in pore-scale.

Three dimensional and real-time pore-level phenomena during water flooding were successfully visualized. To eliminate graphical errors, such as illusory oil/water films, that can be caused by X-ray broadening effects, the oil and water phases were carefully selected so that images produced using the X-ray CT scanner gave separate brightness distributions for each phase. In other words, the brightness of the fluids used bracketed the porous medium brightness. The boundary of each phase could then be determined with high precision, even in a single pore. The shape of the trapped oil and the interface between the water and oil were visualized clearly.

The oil trapping mechanism during water flooding in the upward and downward water injections is nearly the same and is dominated by the water invasion speed differences in some channels. The difference in water invasion speed because of variation of channel size disrupts oil continuity. Discontinued oil blob is trapped inside pore space because interfacial tension prevent its migration. Oil is trapped not only in single pore but also in pore-space clusters. Cluster trapping is possible if the configuration meets the trapping criteria. The size of cluster trapping is mainly determined by the size of water fingers which may occurs due to difference in bouyancy force, difference in viscosity, and variation of channels connected to water displacement front. In the other hand, unique phenomena like snap-off is not a dominant factor for oil trapping process.

The effect of wettability variation of porous media was also observed. In water-wet and oil-wet porous media, piston-like displacement process is the most common oil displacement process. The “overtaking-like” water invasion caused by different water invasion speeds in different channels breaks the continuity of the oil phase. It is the most common oil trapping process in water-wet and oil-wet porous media. In water-wet porous media, an actual water film on the surface of the glass beads was accumulated in the pore throat and snapped-off the continuity of the oil phase. Snap-off process is very rare case

and it is hard to observe the exact moment in 3D porous medium. The contact angle and pore throat radius were measured from direct observations. Those data were used to calculate the capillary pressure during the snap-off and piston-like displacement processes in water-wet and oil-wet porous media. From observation, piston-like displacement is more favorable, because, for a given pore throat radius, the threshold pressure is always higher for piston-like displacement than for snap-off.

In actual oil reservoirs, connate water is usually found. The existence of connate water also significantly affects water flooding and tends to reduce oil recovery by enhancing the instability of the displacement front. In this research, the effect of connate water in water flooding process and oil trapping phenomena was observed. In the porous media without connate water, water flooding was able to produce approximately 1.5 times more oil that in the case of the porous media with connate water. Because of the steady interface movement, the local velocity of oil reduced gradually with time as the water invaded the pore space. The water displacement front was dominated by very large water fingers, leading to better displacement stability. This stable displacement causes water to sweep more area but travel less far at a given time compared with the case of water flooding in a porous media with connate water. When water flooding experiment was conducted in the porous media with connate water, water not only flowed through preexisting connate water, but also occupied neighboring pores. However, less than half of the original oil was produced. When injected water came into contact with connate water contained in pore clusters or with a volume of more than 100 pore spaces, the displacement front suddenly expanded and moved to the end of the connate water channel, leaving the other water fingers behind. Because the pressure gradient was present only in the axial direction toward outlet, this expanding displacement front tended to select pores closest to the outlet. The consequent jump-like movement helped water move faster and reach the outlet earlier than that in the porous media without connate water. Water breakthrough occurred faster so the local velocity of oil was dramatically reduced. The shape of connate water may also deflect the movement of injected water, creating oil entrapment.

After oil has been trapped due to water flooding, injection of sweeping agent is usually conducted by oil company during as part of tertiary production process. In order to release those trapped oil blobs from pore space, sweeping agent (surfactant, bacteria, steam, etc) need to make a contact with the trapped oil blobs. To understand why injection of sweeping agent cannot produce 100% of trapped oil, the flow phenomena around trapped

oil blobs were observed in this research. Three dimensional water flow phenomena around trapped oil blob were visualized by utilizing water doped by NaI as replication of water flooding and pure water as tracer showing its flow pattern around trapped oil blob. In 3D porous media, after water flooding process, injection of additional miscible fluid was able to invade most pores almost homogenously. No significant effect of the existence of trapped oil to deflect the flow field. That additional miscible fluid was able to invade pores located just next to trapped oil. However, in closer inspection, it seems that there is a small amount of stagnant water film comes from water flooding process, that prevent the contact between additional miscible fluid and trapped oil. The size of stagnant water film from water flooding process in unconsolidated packed glass beads case was less than 1 pore size. This stagnant water from water flooding process will act as a barrier preventing the contact between additional miscible fluid and trapped oil blob. In case of surfactant incjection in actual oil reservoir, the stagnant water film surrounding trapped oil blob reduces significantly the effectiveness of surfactant injection. Surfactant will be able to make direct contact with trapped oil blob only by means of molecular diffusion and convection.

REFERENCES

Abramoff, M.D., Magelhaes, P.J., Ram, S.J., Image Processing with ImageJ, Biophotonics International, Vol. 11, No. 7, pp. 36–42 (2004).

Al-Raoush, R.I., Willson, C.S., A pore-scale investigation of a multiphase porous medium system, Journal of Contaminant Hydrology, Vol. 77, No. 1–2, pp. 67–89 (2005).

Amaya, J., Rana, D., Hornof, V., Dynamic Interfacial tension Behavior of Water/Oil Systems Containing In situ-Formed Surfactants, Journal of Solution Chemistry, Vol. 31, No. 2, pp. 139-148 (2002).

Blunt, M., Fayers, F.J., Orr, F.M., Carbon dioxide in enhanced oil recovery, Energy Conversion and Management, Vol. 34, No. 9-11, pp. 1197–1204 (1993).

Blunt, M.J., King, M.J., Simulation and theory of two-phase flow in porous medium, Physical Review A, Vol. 46, No. 12, pp. 7680–7699 (1992).

Blunt, M.J., Scher, H., Pore-level modeling of wetting, Physical Review E, Vol. 52, No. 6, pp. 6387–6403 (1995).

Cinar, Y., Riaz, A., Tchelepi, H.A., Experimental study of CO_2 injection into saline formations, SPE Journal, Vol.14, No.4, pp.588–593 (2009).

Chang, L.C., Tsai, J.P., Shan, H.Y., Chen, H.H., Experimental study on imbibition displacement mechanisms of two-phase fluid using micro model, Environmental Earth Sciences, Vol. 59, No. 4, pp. 901–911 (2009).

Fenwick, D.H., Blunt, M.J., Three-dimensional modeling of three phase imbibition and drainage, Advances in Water Resources, Vol.21, No.2, pp.121–143 (1998).

Goodfield, M., Goodyear, S.G., Townsley, P.H., New Coreflood Interpretation Method for Relative Permeabilities Based on Direct Processing In-Situ Saturation Data, The 2001 SPE Annual Technical Conference and Exhibition, SPE 71490 (2001).

Graue, A., Fernø, M.A., Aspenes, E., Needham, R., Wettability effects on water mixing during waterflood oil recovery, Journal of Petroleum Science and Engineering, Vol. 94–95, pp. 89–99 (2012).

Graue, A., Fernø, M.A., Water mixing during spontaneous imbibition at different boundary and wettability conditions. Journal of Petroleum Science and Engineering, Vol. 78, No. 3–4, pp. 586–595 (2011).

Jamaloei, B.Y., Asghari, K., Kharrat, R., Ahmadloo, F., Pore-scale two-phase filtration in imbibition process through porous medium at high- and low-interfacial tension flow condition, Journal of Petroleum Science and Engineering, Vol. 72, No. 3–4, pp. 251–269 (2010).
Jamaloei, B.Y., Kharrat, R., Pore-scale description of surfactant-enhanced waterflooding for heavy oil recovery, Journal of Petroleum Science and Engineering, Vol. 92, pp. 89–101 (2012).

Jerauld, G.R., Salter, S.J., The effect of pore-structure on hysteresis in relative permeability and capillary pressure: pore-level modeling, Transport in Porous Medium, Vol. 5, No. 2, pp. 103–151 (1990).

Kang, Q., Zhang, D., Chen, S., Immicible displacement in a channel: simulations of fingering in two dimensions, Advances Water Resources, Vol. 27, No. 1, pp. 13–22 (2004).

Kumar, M., Knackstedt, M.A., Senden, T.J., Sheppard, A.P., Middleton, J.P., Visualizing and quantifying the residual phase distribution in core material, Petrophysics, Vol. 51, No. 5, pp. 323–332 (2010).

Kang, Q., Zhang, D., Chen, S., Immicible displacement in a channel: simulations of fingering in two dimensions, Advance in Water Resources, Vol.27, No. 1, pp.13–22 (2004).

Kestin, J., Sokolov, M., Wakeham, W.A., Viscosity of liquid water in the range -8ºC to 150ºC, Journal of Physical and Chemical Reference Data, Vol. 7, No. 3, pp. 941–948 (1978).

Lake, L. W., 1989. Enhanced Oil Recovery. New Jersey: Prentice Hall.

Lenormand, R.: Liquids in porous medium. Journal of Physics : Condensed Matter, Vol. 2, No. SA79–SA88 (1990).

Lenormand, R., Touboul, E., Zarcone, C., Numerical models and experiments on immiscible displacements in porous medium, Journal of Fluid Mechanics, Vol. 189, pp. 165–187 (1988).

Lenormand, R., Capillary fingering: percolation and fractal dimension, Transport in Porous Medium, Vol. 4, pp. 599–612 (1989).

Lenormand, R., Touboul, E., Zarcone, C., Numerical models and experiments on immiscible displacements in porous medium, Journal of Fluid Mechanics, Vol. 189, pp. 165–187 (1988).

Lindquist, W.B., Venkatarangan, A., Investigating 3D geometry of porous medium form high resolution images, Physics and Chemistry of the Earth (A), Vol. 25, pp. 593–599 (1999).

Løvoll, G., et al., Competition of gravity, capillary and viscous forces during drainage in a two-dimensional porous medium, a pore scale study, Energy, Vol. 30, pp. 861-872 (2005).

Morrow, N.R., Mason, G., Recovery of oil by spontaneous imbibition. Current Opinion in Colloid & Interface Science, Vol. 6, pp. 321–337 (2001).

Morrow, N.R., Songkran, B., Effect of viscous and buoyancy forces on nonwetting phase trapping in porous medium. In: D. O. Shah (Ed.), Surface Phenomena in Enhanced Oil Recovery, Plenum Press (1981), pp. 387–411.

Paterson, L., Hornof, V., Neale, G.H., Water fingering into an oil-wet porous medium saturated with oil at connate water saturation, J. Rev. Inst. Fr. Pet., Vol. 39, No. 4, pp. 517–521 (1984).

Porzucek, C., Ramires, W.F., Optimal injection strategies for surfactant flooding enhanced oil recovery, part 1 – results using streamtube reservoir simulation, Journal of Petroleum Science and Engineering, Vol. 4, No. 4, pp. 323–334 (1990).

Rasband, W.S.: Image J, National Institute of Health, Bathesda, Maryland, USA, http://rsbweb.niih.gov/ij/, (1997-2008)

Saffman, P.G., Taylor, G.I., The penetration of a fluid into a porous medium Hele-Shaw cell containing a more viscous liquid, Proc R Soc London A, Vol. 245, No. 1242, pp. 312–329 (1958).

Suekane, T., Tezuka, R., Pore-scale observation of surfactant flooding for weakly water-wet porous media: the effect of gas injection to improve oil recovery, In: Computational Methods in Multiphase Flow VII, (ed.) CA. Brebbia, P. Vorobieff, WIT-Press, (2013), pp.487–497.

Wildenscheld, D., Hopmans, J.W., Vaz, C.M.P., Rivers, M.L., Rikard, D., Using X-ray computed tomography in hydrology: systems, resolutions, and limitations, Journal of Hydrology, Vol.267, pp.285–297 (2002).